Dedicated to innovation in aerospace

NLR-TP-2015-019 | May 2017

Strength of notched and un-notched thermoplastic composite laminate in biaxial tension and compression

CUSTOMER: National Aerospace Laboratory NLR

NLR – Netherlands Aerospace Centre

Netherlands Aerospace Centre

NLR is a leading international research centre for aerospace. Bolstered by its multidisciplinary expertise and unrivalled research facilities, NLR provides innovative and integral solutions for the complex challenges in the aerospace sector.

NLR's activities span the full spectrum of Research Development Test & Evaluation (RDT & E). Given NLR's specialist knowledge and facilities, companies turn to NLR for validation, verification, qualification, simulation and evaluation. NLR thereby bridges the gap between research and practical applications, while working for both government and industry at home and abroad.

NLR stands for practical and innovative solutions, technical expertise and a long-term design vision. This allows NLR's cutting edge technology to find its way into successful aerospace programs of OEMs, including Airbus, Embraer and Pilatus. NLR contributes to (military) programs, such as ESA's IXV re-entry vehicle, the F-35, the Apache helicopter, and European programs, including SESAR and Clean Sky 2.

Founded in 1919, and employing some 650 people, NLR achieved a turnover of 71 million euros in 2016, of which three-quarters derived from contract research, and the remaining from government funds.

For more information visit: **www.nlr.nl**

Dedicated to innovation in aerospace

Strength of notched and un-notched thermoplastic composite laminate in biaxial tension and compression

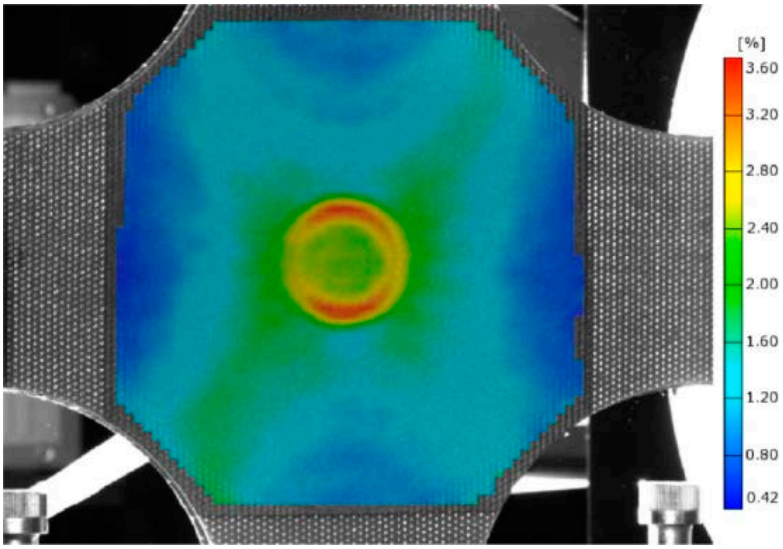

Figure: Aramis von Mises strains in the cruciform specimen in a biaxial tension-tension test.

Problem area

Modern composite laminates offer large advantages for the design and development of aircraft structures, for example by their local anisotropic properties and by their greatly enhanced strength-to-weight and stiffness-to-weight ratios. In particular, thermoplastic composites have additional benefits, among others due to their improved toughness, impact resistance, damage tolerance, reparability and manufacturability.

Description of work

The present study investigates the static strength of notched and un-notched 8-ply quasi-isotropic thermoplastic carbon composite laminate under in-plane biaxial loading. The specimen used in this study is based on the cruciform designs

REPORT NUMBER
NLR-TP-2015-019

AUTHOR(S)
W.J. Vankan
B.H.A.H. Tijs
G.J. de Jong
H.C. de Frel
N.K. Singh

REPORT CLASSIFICATION
UNCLASSIFIED

DATE
May 2017

KNOWLEDGE AREA(S)
Computational Mechanics and Simulation Technology

DESCRIPTOR(S)
quasi-isotropic laminate
failure test
coupons
finite element model

proposed and successfully used in previous studies. The specimen consists of a central thermoplastic composite laminate of carbon-fibre reinforced polymer (CFRP), with large composite tabs of glass-fibre reinforced polymer (GFRP) attached on both sides of the laminate.

Results and conclusions

A biaxial test program covering various biaxial load combinations in tension-tension, tension-compression and compression-compression has been successfully executed and biaxial failure values have been determined. It was found that the biaxial load-case with at least one compression component, buckling or bending of the laminate in the central test section of the specimen was very critical. Therefore an anti-buckling guide (ABG) was successfully designed and applied in the biaxial tension-compression and compression-compression load-cases. A small area of the test-section remained unsupported by the ABG to allow for the DIC strain measurements with the Aramis DIC system.

Besides the experimental biaxial test program, also FE modelling and analyses are used, both to predict the global outcomes of the biaxial tests and to interpret the test results. From the Aramis DIC system, failure loads and strains have been obtained. Failure stresses have been determined by either scaling the failure load to the linear portion of the load-strain relations or by directly considering the failure strain recorded by Aramis. The stresses have been used to construct failure envelopes for the plain and open-hole specimens. For both envelopes it is concluded that good agreement is found between the theoretically predicted envelopes and the data from the tests. This confirms that the general failure criteria, which have been primarily developed for thermoset material, are also valid for thermoplastic material and that thermoplastic specific properties do neither adversely affect the current failure theories, nor that effects are missed in those criteria.

Applicability

Based on the findings given in this report it is expected that composite parts with lower weight can be made as compared to parts that are designed with the previous uni-axially based failure criteria.

NLR
Anthony Fokkerweg 2
1059 CM Amsterdam
p) +31 88 511 3113 f) +31 88 511 3210
e) info@nlr.nl i) www.nlr.nl

Dedicated to innovation in aerospace

NLR-TP-2015-019 | May 2017

Strength of notched and un-notched thermoplastic composite laminate in biaxial tension and compression

CUSTOMER: National Aerospace Laboratory NLR

AUTHOR(S):

W.J. Vankan	Nationaal Lucht- en Ruimtevaartlaboratorium
B.H.A.H. Tijs	Fokker Aerostructures
G.J. de Jong	Nationaal Lucht- en Ruimtevaartlaboratorium
H.C. de Frel	Fokker Aerostructures
N.K. Singh	Fokker Aerostructures

NLR - Netherlands Aerospace Centre

This report is based on a paper published in Journal of Composite Materials, Vol. 50(25), 3477–3500, 2016, by SAGE Publications Ltd. http://journals.sagepub.com/doi/full/10.1177/0021998315621963.

CUSTOMER	**National Aerospace Laboratory NLR**
CONTRACT NUMBER	**- - -**
OWNER	**NLR**
DIVISION NLR	**Aerospace Vehicles**
DISTRIBUTION	**Unlimited**
CLASSIFICATION OF TITLE	**UNCLASSIFIED**

APPROVED BY :		
AUTHOR	**REVIEWER**	**MANAGING DEPARTMENT**
W.J. Vankan	B.A.T. Noordman	A.A. ten Dam
DATE 22 05 17	DATE 22 05 17	DATE 22 05 17

Summary

Composite laminates are being increasingly used in a wide variety of industrial applications, but there are difficulties in applying these materials in ways that exploit their full potential, in particular under multi-axial loading. The objective of the present study is to determine by experiments the biaxial failure data for composite laminates produced by Fokker Aerostructures based on the thermoplastic UD carbon reinforced material AS4D/PEKK-FC. A test machine and accompanying cruciform specimens for in-plane biaxial failure tests have been developed. A coupon-level biaxial test program covering various biaxial load combinations in tension-tension, tension-compression and compression-compression has been successfully executed and biaxial failure values for the thermoplastic laminate have been determined.

Besides the experimental biaxial test program, also finite element models and analyses have been used to predict the global outcomes of the biaxial tests and to interpret the test results. Both plain (un-notched) and open-hole (notched) specimens of the thermoplastic laminate have been tested. The biaxial failure data have been collected and further processed in biaxial failure criteria. From the experiments, the failure strains, stresses and loads are determined and a failure envelope is created for both plain and open-hole specimens. Good agreement is found between the theoretically predicted envelopes and the test data.

From the findings for biaxial failure criteria from this study it is expected that structural weight saving can be achieved in the design of multi-axially loaded composite parts as compared to the design with the previous uni-axially based failure criteria.

This page is intentionally left blank.

Strength of notched and un-notched thermoplastic composite laminate in biaxial tension and compression

Wilhelmus J Vankan[1], Bas HAH Tijs[2], Gerrit J de Jong[3], Herman C de Frel[2] and Niels K Singh[2]

Abstract

Composite laminates are being increasingly used in a wide variety of industrial applications, but there are difficulties in applying these materials in ways that exploit their full potential, in particular under multi-axial loading.

The objective of the present study is to determine by experiments the biaxial failure data for composite laminates produced by Fokker Aerostructures based on the thermoplastic UD carbon reinforced material AS4D/PEKK-FC.

A test machine and accompanying cruciform specimens for in-plane biaxial failure tests have been developed. A coupon-level biaxial test program covering various biaxial load combinations in tension-tension, tension-compression and compression-compression has been successfully executed and biaxial failure values for the thermoplastic laminate have been determined.

[1]Collaborative Engineering Systems Department, National Aerospace Laboratory NLR, Amsterdam, The Netherlands
[2]Engineering Department, Fokker Aerostructures, Papendrecht, The Netherlands
[3]Structures Testing & Evaluation Department, National Aerospace Laboratory NLR, Marknesse, The Netherlands

Corresponding author:
Wilhelmus J Vankan, Collaborative Engineering Systems Department, National Aerospace Laboratory NLR, PO Box 90502, 1006 BM, Amsterdam, The Netherlands.
Email: jos.vankan@nlr.nl

Besides the experimental biaxial test program, also finite element models and analyses have been used to predict the global outcomes of the biaxial tests and to interpret the test results.

Both plain (un-notched) and open-hole (notched) specimens of the thermoplastic laminate have been tested. The biaxial failure data have been collected and further processed in biaxial failure criteria. From the experiments, the failure strains, stresses and loads are determined and a failure envelope is created for both plain and open-hole specimens. Good agreement is found between the theoretically predicted envelopes and the test data.

From the findings for biaxial failure criteria from this study it is expected that structural weight saving can be achieved in the design of multi-axially loaded composite parts as compared to the design with the previous uni-axially based failure criteria.

Keywords

Quasi-isotropic laminate, failure test, coupons, finite element model

Introduction

Modern composite laminates offer large advantages in comparison to metals for the design and development of aircraft structures, for example by their local anisotropic properties and by their greatly enhanced strength-to-weight and stiffness-to-weight ratios.[1] In particular, thermoplastic composites have additional benefits, among others due to their improved toughness, impact resistance, damage tolerance, reparability and manufacturability.[2]

Aircraft structures are loaded multi-axially and material failure is one of the driving design criteria in the structural design process. Detailed knowledge of the strength properties of composite laminates under multi-axial loading is therefore a research topic which is of paramount importance.[3] Static strength properties are commonly evaluated by conventional static coupon tests with uni-axial

loading.[4] Due to their anisotropic nature, the static strength of composite laminates under multi-axial loading strongly depends on the applied load combination. The understanding of the behaviour of composite laminates under multi-axial loading is of great practical significance, since bi- or even tri-axial loading regimes are the norm in real engineering structures. Composite material failure is therefore subject of extensive study. For example, a recent extensive review of composite material failure models, including discussions of the various reviewed theories, was published in 2008 by Orifici et al.[5] They presented many different criteria, roughly from the literature from the past four decades, e.g. based on fibre failure, matrix failure, or fibre-matrix shear failure, and criteria for ply failure and delamination onset and –growth. However, a single unified failure theory that can accurately predict the initial onset and final failure of a general laminate under general loading is lacking, as appeared in the 2004 World-Wide Failure Exercise (WWFE),[3] where also the scarcity of reliable experimental data for bi-axially (2-D) and tri-axially (3-D) loaded composites was exposed. Nevertheless, various biaxial test procedures have been designed and applied in the past decades, mostly limited to biaxial tension only.[6]

One effective method to measure biaxial mechanical properties of composite laminates is through in-plane biaxial testing using cruciform specimens. In an early specimen design study finite element method (FEM) calculations on different cruciform specimen geometries and some different materials were done to determine which specimen design yielded the most suitable biaxial stress distribution.[7,8] These cruciform specimens had a reduced thickness in the central test section. The behaviour of the specimens was investigated for isotropic aluminium (AL-2024-T3), graphite-epoxy (T300/N5208) and graphite-PEEK (AS4/PEEK) materials with $[45/0/-45/0]_s$ lay-ups. On the cruciform arms, plies of the same material were added with various layups of $[0/90]_{ns}$, $[+15]_{ns}$, $[+30]_{ns}$, $[+45]_{ns}$ and $[45/-45]_{ns}$. The resulting most suitable cruciform specimen design was adopted in[9] to experimentally determine the biaxial strength of quasi-isotropic (QI) laminate (carbon fibre/180^{o}C cured epoxy HTA/#101) with a $[0/90/45/-45]_s$ lay-up and a thickness of 1 mm in biaxial tension-tension and tension-compression tests. In the study presented in,[9] glass fibre laminate tabs were

bonded on the carbon laminate to reinforce the arms and FEM simulations were performed, which showed the intended stress concentration in the central gauge section. Experiments were successfully performed to determine the failure loads in tension-tension and tension-compression. High speed camera images showed that failure was initiated in the central specimen gauge section.

The cruciform specimen design proposed in[8] was also adopted in more recent experimental studies[10,11] where among others the effects of open-hole on biaxial failure strength was investigated. In[10] a quasi-isotropic ($[0/45/90/-45]_s$) carbon composite (Hexcel IM7/8552 unidirectional prepreg) laminate core with a nominal thickness of 2 mm was considered. Similar as in[9,11] this carbon laminate was bonded between two large glass fibre (G10 woven) tabs (Figure 1). Plain and open-hole (10 mm diameter) specimens were successfully tested in,[10] but the biaxial load ratios were limited to only tension-tension and tension-compression.

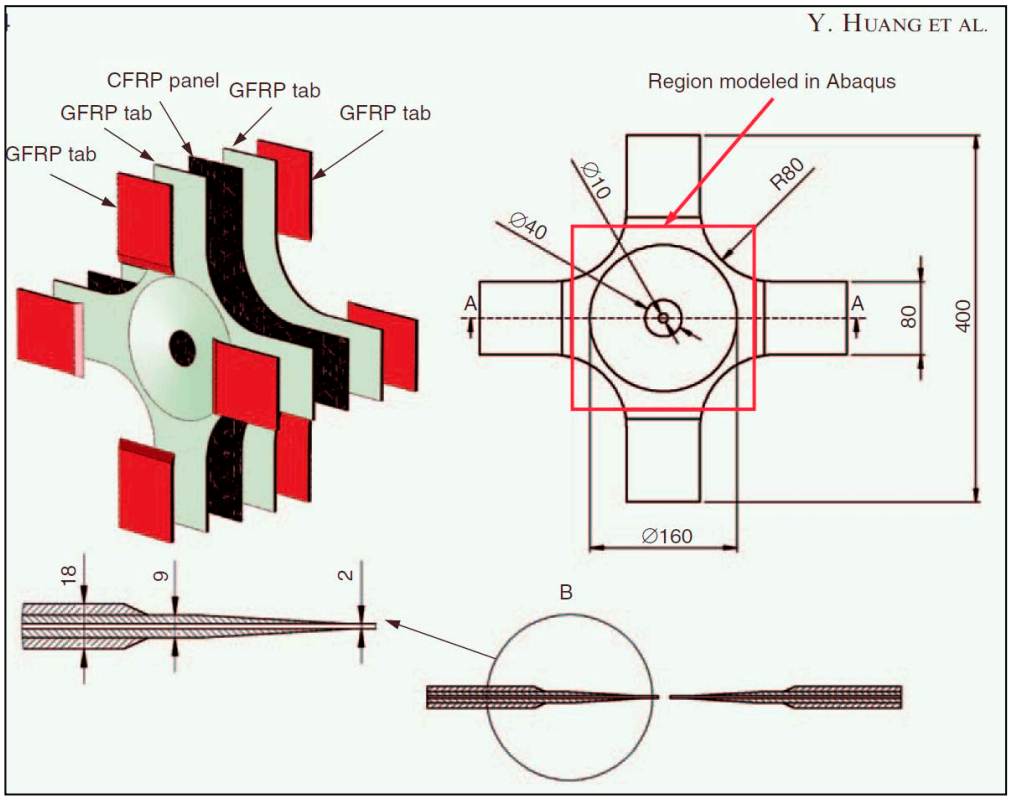

Figure 1. Illustration of the design and sizing of the cruciform coupon used by Huang et al.[10] The coupon consists of a central carbon-fibre composite (CFRP) layer with large glass-fibre composite (GFRP) tabs attached on both sides of the laminate.

Just like in,[9,10,11] the specimen used in this study is also based on the cruciform design proposed in[8] and also the static strength is determined for plain and open-hole (un-notched and notched) quasi-isotropic carbon composite laminates under in-plane biaxial loading. In addition to the biaxial load ratios tension-tension and tension-compression considered in,[10,11] now also biaxial compression-compression loading is considered. The biaxial test machine and cruciform specimen design were specifically developed for these tests. In total 28 biaxial tests under various biaxial load-ratios were successfully performed, from which the static strength values were determined. Recordings were made of the specimen arm loads and of the local laminate failure strains using digital image correlation (DIC) strain measurements. These static strength values were used for the validation and further development of a biaxial failure model for the considered laminate.

Specimen design and production

The present study investigates the static strength of notched and un-notched 8-ply quasi-isotropic ($[45/0/-45/90]_s$) thermoplastic carbon composite laminate under in-plane biaxial loading. The specimen used in this study is based on the cruciform designs proposed in Suzuki and Ishikawa and Huang et al.[8,10] The specimen consists of the central carbon-fibre reinforced polymer (CFRP) composite laminate (about 1.1mm thick; 8 plies) with large glass-fibre reinforced polymer (GFRP) composite tabs attached on both sides of the laminate. The ply properties of the thermoplastic CFRP material (Cytec AS4D/PEKK-FC) are given in Table 1.

Table 1. Ply properties of AS4D/PEKK-FC.

Property	Value
Ply thickness: t_{ply} [mm]	0.14
Longitudinal stiffness: E_{11} [MPa]	139000
Transverse stiffness: E_{22} [MPa]	10300
Shear stiffness: G_{12} [MPa]	5200
Poisson's ratio: ν_{12} [-]	0.3
Longitudinal tensile strength: f_1^t [MPa]	2463
Longitudinal compressive strength: f_1^c [MPa]	-1493
Transverse tensile strength: f_2^t [MPa]	61
Transverse compressive strength: f_2^c [MPa]	-254

Longitudinal shear strength: f_{12} [MPa]	100

The cruciform specimen in this study shall have a gauge section diameter of about 31.8mm. The notched cruciform specimen shall have an open-hole diameter of about 6.35mm, to be applied in the centre of the circular gauge section. The final sizing of the cruciform specimen is achieved by determining suitable values for the two design variables of the specimen: the cruciform radius R and the tab thickness t_{tab} (see Figure 2). These design variables have been determined using linear finite element (FE) analyses. The FE model that was used in these analyses will be described in a separate section below. The specimen sizing is such that the maximum stresses occur in the central test section of the specimen (i.e. in the CFRP laminate) and such that the estimated CFRP laminate failure stress level of about 1 GPa is achieved in the test section with arm loads that are less than 200kN, i.e. the arm loads that must be feasible with the test machine. The estimated CFRP laminate failure stress level is based on un-notched uni-axial coupon tests. The resulting suitable values that were found for the design variables of the specimen are a cruciform radius R of 70mm and the tab thickness t_{tab} of 6mm (see Figure 2).

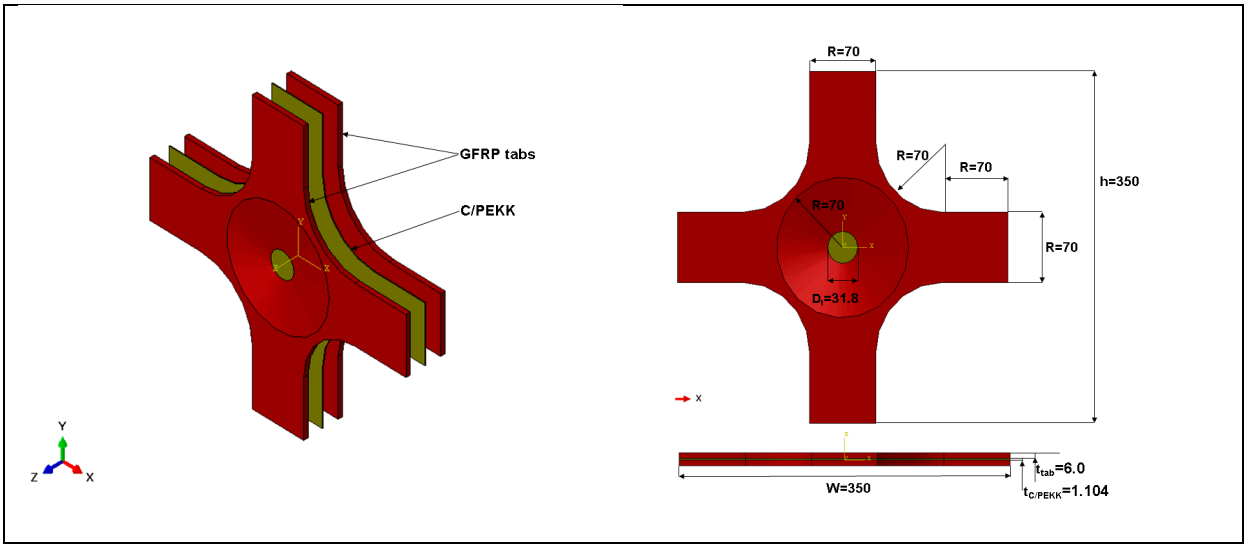

Figure 2. Final design and sizing of the cruciform specimen for the biaxial tests.

Each cruciform specimen is composed by secondary bonding of one CFRP and two GFRP cruciform parts. First the cruciform contours of the CFRP and GFRP parts are precision-machined out of CFRP laminate plates of about 360mm x 360mm, 1.13 mm thick (mean value over all specimens; the theoretical 8 ply thickness is 1.12mm), and GFRP laminate plates of about 360mm x 360mm, 6mm thick. Then the 31.8mm diameter hole for the central gauge section and the 140mm outer-diameter central conical-tapered section are precision-machined in the GFRP parts. The machined CFRP and GFRP cruciform parts are prepared by proper cleaning and de-greasing of the bonding surfaces. Bonding film (3M™ Scotch-Weld™ Structural Adhesive Film AF 163-2 3M) sheets are cut in cruciform shape, then accurately positioned together with the CFRP and GFRP parts and all edges sealed with Flashbreaker 2 foil (3M™ High Temperature Aluminum Foil Tape 433). Then the specimen assembly is carefully vacuum-bagged and cured in 2 consecutive cycles of about 3hrs autoclave at 125^{o}C and 1.4 bar. Because of the high cost of the manufacturing of the specimens, only a rather limited number of 28 specimens in total could be produced in the present study. Of these specimens, 14 are kept as plain (un-notched; see Figure 3) and the other 14 are prepared as notched specimens by drilling a 6.35mm diameter open-hole in the centre of the gauge section.

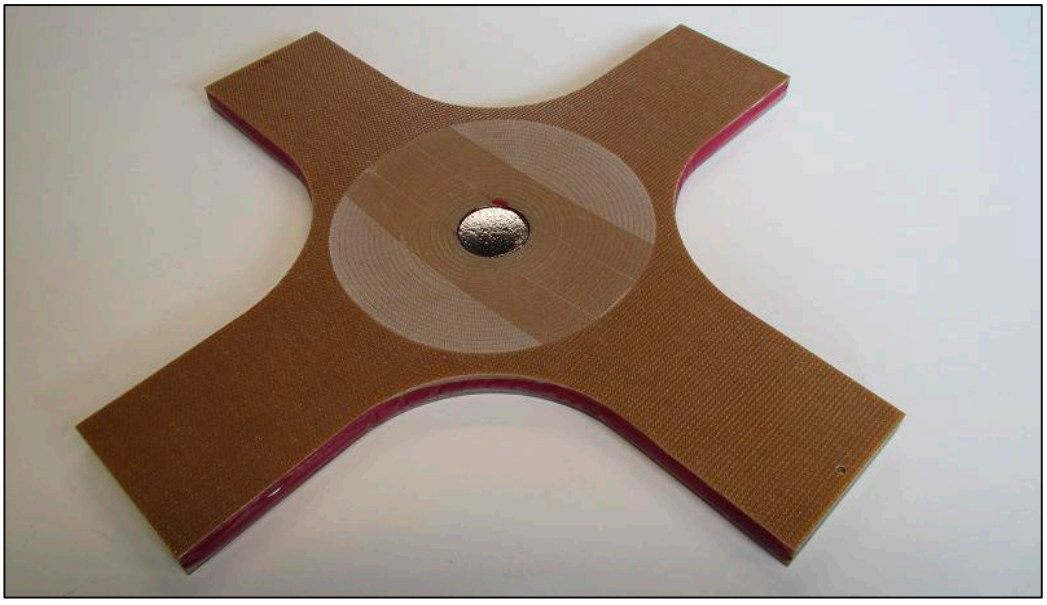

Figure 3. Photograph of the plain (un-notched) cruciform specimen produced in this study.

For strain measurements, all specimens were prepared for one-sided Aramis[12] DIC measurements with a standard speckle pattern. On a small sub-set of the un-notched specimens, also 45° strain gauge rosettes (Micro Measurements stacked rosette type WA-06-120WR-350[13]), were fixed in the centre of the test section, giving the local strain values for ε_1, ε_2, ε_{45}, measured in the laminate's 0°, 90° and 45° directions, respectively.

Biaxial test machine

In accordance with the aims of the study to investigate composite laminate failure in planar biaxial tensile and compressive load states, a test rig for biaxial failure testing of composite laminates was developed. Several concepts for the test rig have been evaluated, first leading to an initial design for a horizontal loading frame and eventually to the final design of the complete test rig. The final test rig design is based on the concept where the vertical loading axis is a conventional vertical uni-axial testing machine and the horizontal loading axis is force-free suspended, i.e. is not fixed but moves with the deforming coupon. This concept was found to be applied successfully in the past, e.g. in biaxial fatigue testing of metallic coupons[14] (Figure 4).

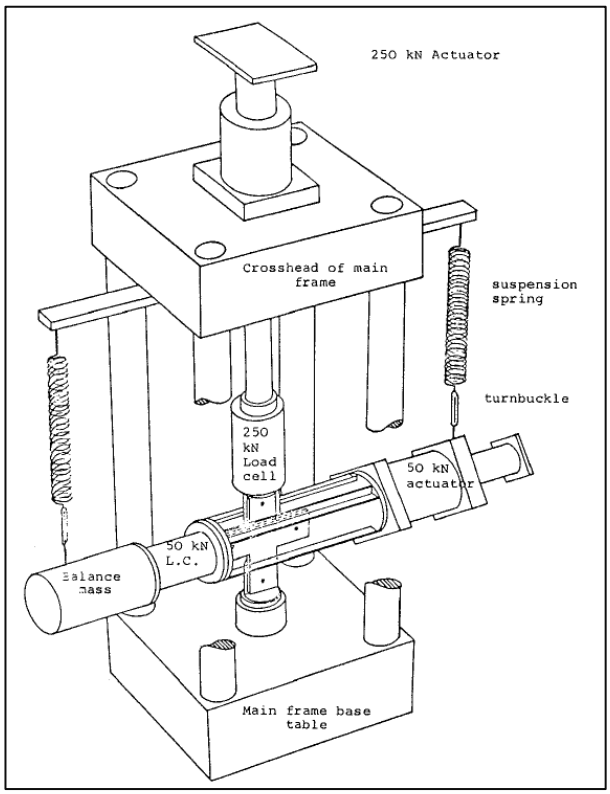

Figure 4. Example of biaxial test rig with force-free suspended horizontal loading axis as applied by Charvat and Garrett.[14]

The design of the NLR biaxial test machine is mainly concerned with the frame and suspension of the horizontal loading axis. This horizontal loading frame is mounted by vertical suspension springs in the 500kN MTS dynamic test rig (MTS type MTS328.41[15]), much like the test set-up as presented in.[14] The horizontal loading frame comprises mainly:

- 2 hydrostatic symmetrical double acting actuators[16], max. stroke 300mm, 100kN each;
- stiff steel connection beams;
- 2 load-cells,[17] type 1220-25klbf;
- 2 hydraulic grips,[18] max. 200kN both in tension and compression;
- 2 vertical suspension springs, each with a stiffness of 11kN/m;
- a steel frame, mounted on top of the MTS test rig, from which the horizontal loading frame is suspended.

The horizontal loading frame, including the hydraulic actuators, grips, hoses and couplings, weighs in total about 500kg. The vertical suspension is achieved through steel tension springs of about 0.5m

long and chain hoists for global vertical positioning of the horizontal loading frame. The stiffness of the suspension springs of about 11kN/m, yields a spring extension due to the horizontal loading frame of about (500x9.81 N)/(2x11000 N/m) = 0.223m, and “parasitic” vertical forces on the coupon may occur of about 22N for each mm of movement of the horizontal loading frame away from the force-free suspended vertical position. As these movements are expected to not be more than a few mm, the resulting parasitic vertical forces are expected to remain below 100N maximum, which is quite acceptable when taking into account that the coupon arm forces in the tests are expected to be in the order of 100kN at coupon failure.

The feasible arm loads in the coupon that can be achieved by the biaxial test rig are currently mainly limited by the hydraulic grips that are used in the rig, which have maximum load capacities of roughly 200kN for the horizontal axis and 500kN for the vertical axis. The resulting design of the NLR biaxial test rig is illustrated in the Figure 5.

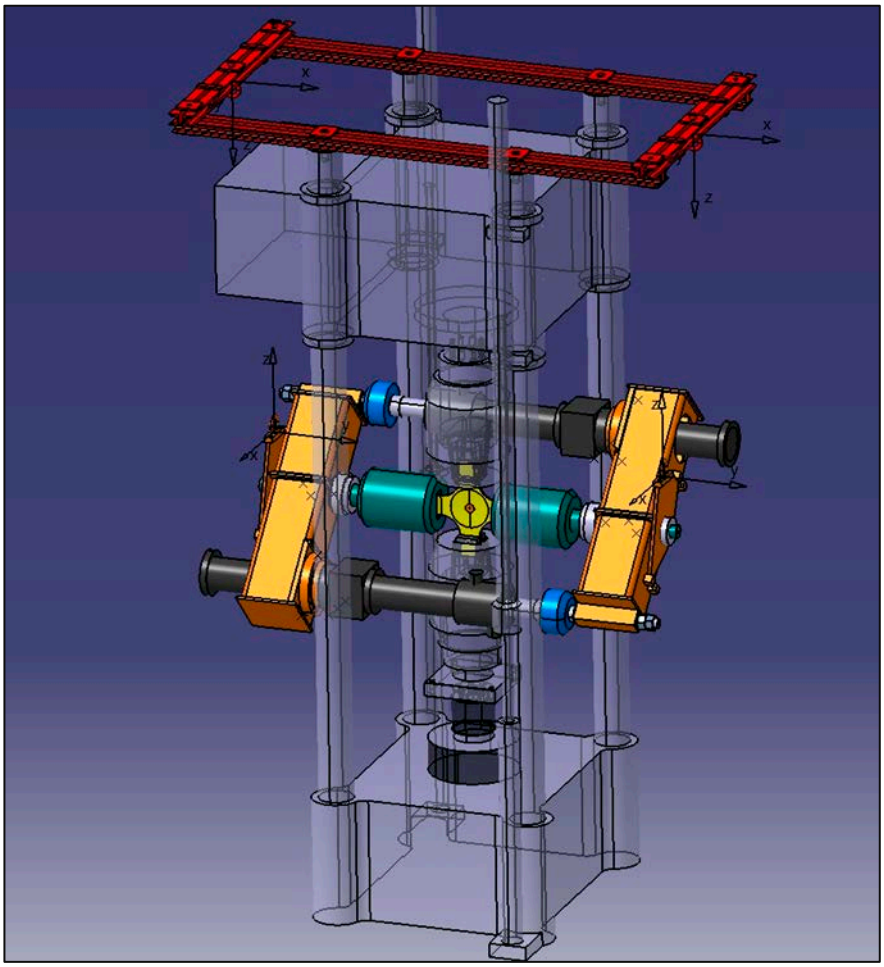

Figure 5. Design of the biaxial test rig. The horizontal loading frame (coloured parts) is mounted in the MTS dynamic test rig (semi-transparent parts) by vertical suspension springs (not shown here). The coloured parts represent the steel frame on top (in red), the hydrostatic double acting actuators (in black), the stiff steel connection beams (in orange), the 2 load-cells (in blue), the hydraulic grips (in green) and steel connection components (in bright grey); the specimen is shown in yellow.

According to this design, the NLR biaxial test rig has been realized as illustrated in the test set-up shown in Figure 6 and Figure 7.

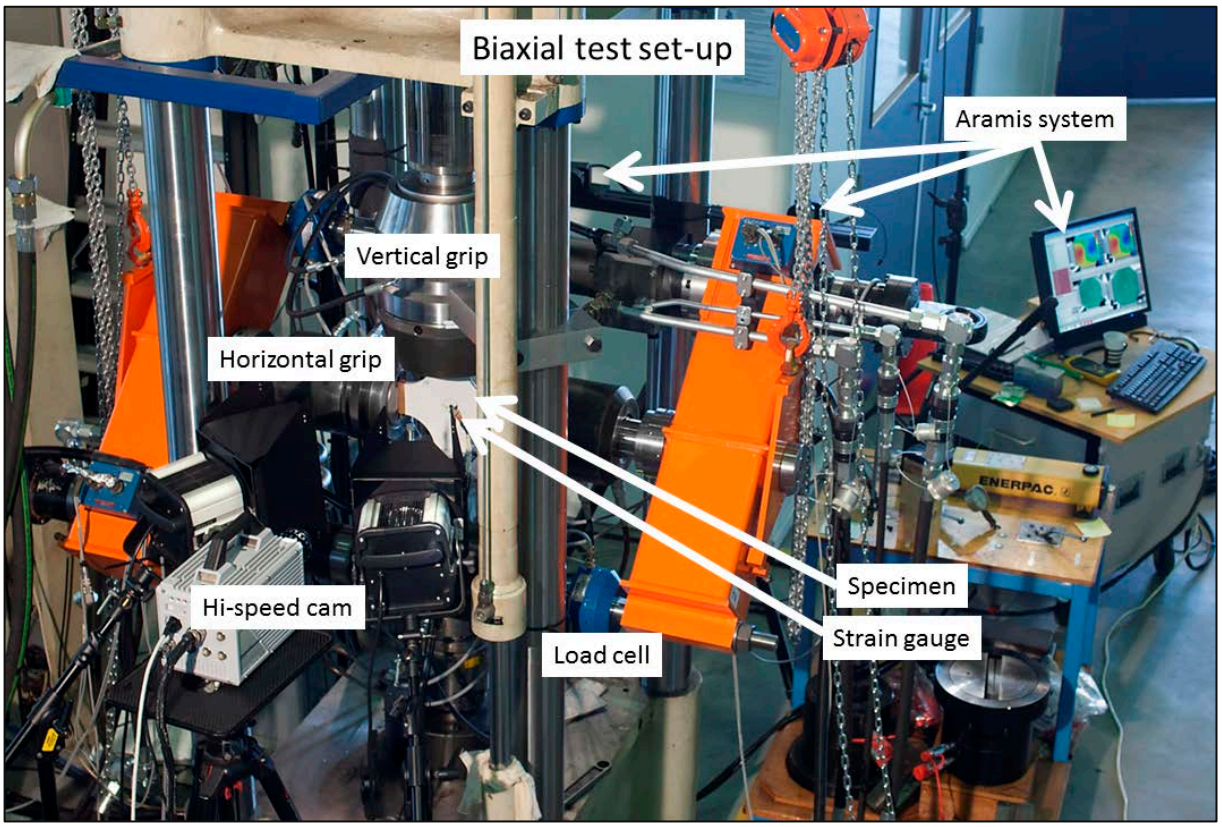

Figure 6. Overview of the biaxial test set-up.

The test set-up shown above is applied for the biaxial tension-only tests (i.e., only tension-tension tests). For the compression tests (i.e., tension-compression or compression-compression tests) an anti-buckling guide (ABG) must be applied to prevent the out-of-plane bending or buckling of the test section under the compressive loading. This ABG is specifically designed and built for the cruciform specimens, and its deployment in a compression-compression test is shown in the Figure 7. The ABG consists of two concentric teflon-coated steel rings that are pressed on both sides of the specimen surface. Two different types of ABG rings have been used during testing: closed rings (suppressing all central out-of-plane displacements) and open rings (allowing visibility on central region for Aramis system), as illustrated in Figure 8.

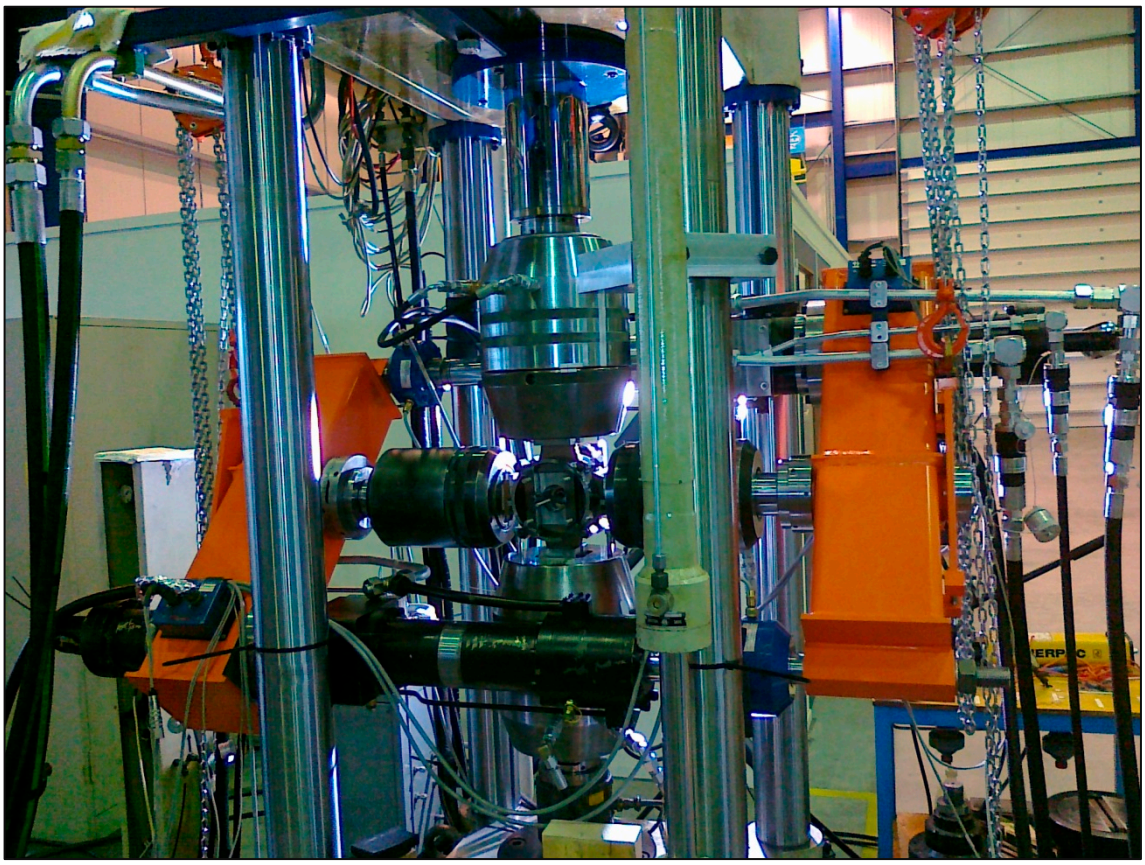

Figure 7. Test set-up for compression tests (in this case compression-compression) where an ABG (in centre of the picture) is applied to prevent the out-of-plane bending or buckling of the test section.

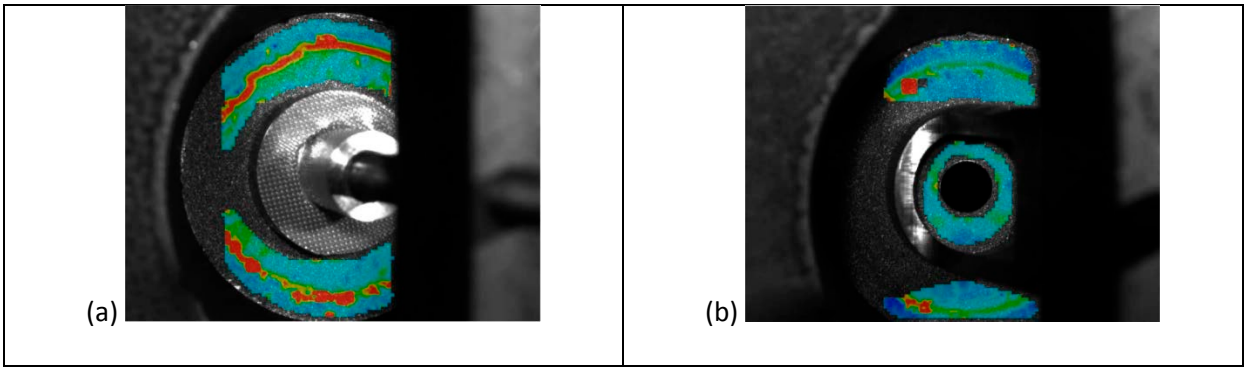

Figure 8. Two different types of anti-buckling guides are used: (a) with closed rings and (b) open rings. (The colour patterns are from Aramis strain recordings)

Finite element model and predictions

For a global understanding of the behaviour of the specimens in the biaxial tests, various FEM analyses of the biaxial tests are performed. The analyses are meant for investigations of the effects

and trends occurring in the various biaxial tests, taking into account the actual geometry (in-plane and thickness) of the specimen. Therefore these analyses are limited to linear static FEM analyses using linear elastic material behaviour. For the global specimen failure estimation, the effective in-plane failure stress (based on uni-axial coupon tests) of the 8-ply quasi-isotropic CFRP laminate is considered (Table 2). Hence the FE model is limited to homogenized in-plane-isotropic material properties of the laminate. To account also for out-of-plane effects due to the thickness variations in the geometry of the GFRP tabs and due to the compression forces of the grips on the arms of the cruciform, a 3D FE model of the specimen with 3D quadratic elements is used. The homogenized 3D effective orthotropic material properties for the CFRP and GFRP laminates that were used in the FE analyses are specified in Table 2. Note that the out-of-plane properties for the laminates were not exactly known and therefore quite conservative (low) values were used. From various analyses it was also found that these values play a minor role because the specimen behaviour is dominated by its in-plane properties.

Table 2. CFRP and GFRP laminates effective material properties.

CFRP 8 ply QI laminate effective properties (UD AS4D-PEKK-FC)	
Property	value
Layup [-]	$[45/0/-45/90]_s$
Thickness [mm]	8x0.14 mm = 1.12 mm
E_{11} [MPa]	54000
E_{22} [MPa]	54000
E_{33} [MPa]	3500
G_{12} [MPa]	20600
G_{23} [MPa]	3500
G_{13} [MPa]	3500
v_{12} [-]	0.31
v_{23} [-]	0.31
v_{13} [-]	0.31
in-plane strength for un-notched tension failure: f_u^t [MPa]	860

GFRP n-ply laminate effective properties (glass–fiber/polyetherimide - glass/PEI)	
Property	value
Layup [-]	$[0/90]_n$ woven plies
ply thickness [mm]	0.24mm
E_{11} [MPa]	18000
E_{22} [MPa]	18000
E_{33} [MPa]	3500
G_{12} [MPa]	3500
G_{23} [MPa]	3500
G_{13} [MPa]	3500
v_{12} [-]	0.3
v_{23} [-]	0.3
v_{13} [-]	0.3
in-plane strength for un-notched tension failure: f_u^t [MPa]	300

in-plane strength for notched tension failure: f_n^t [MPa]	443

The global specimen FE model is developed in ABAQUS CAE 6.12[19] and consists of three parts, see Figure 9: the central CFRP laminate (black), the GFRP conical tabs (red) and steel (isotropic, E=200GPa, v=0.3) blocks of 4mm thick (grey) that represent the grips of the test rig. The global specimen model assembly comprises the CFRP laminate part instance, two GFRP conical tab part instances and eight steel block part instances (Figure 9). All part instances are fixed together with tie constraints. Besides the in-plane biaxial forces, this model also considers the compressive force of the hydraulic grips i.e. applied on the steel blocks upper faces, which is assumed constant and equal to the maximum in plane force (i.e. about 200 kN). For efficiency, the symmetry in the X, Y and Z centre-planes of the geometry, properties and boundary conditions of the global specimen model is exploited and the analyses are performed on one-eighth (1/8) of the whole geometry, as indicated in the Figure 9.

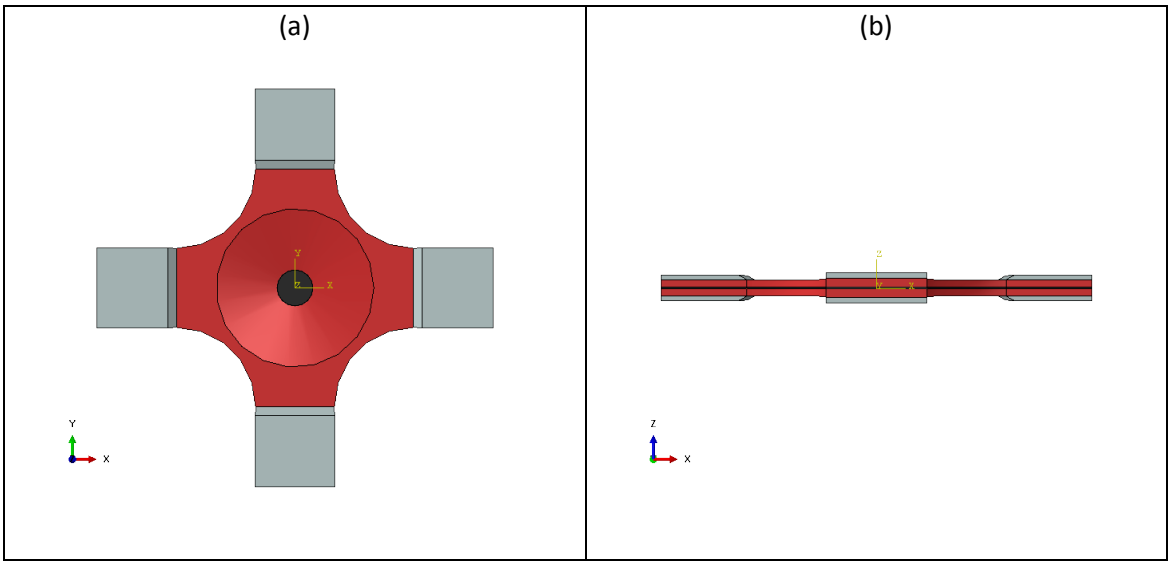

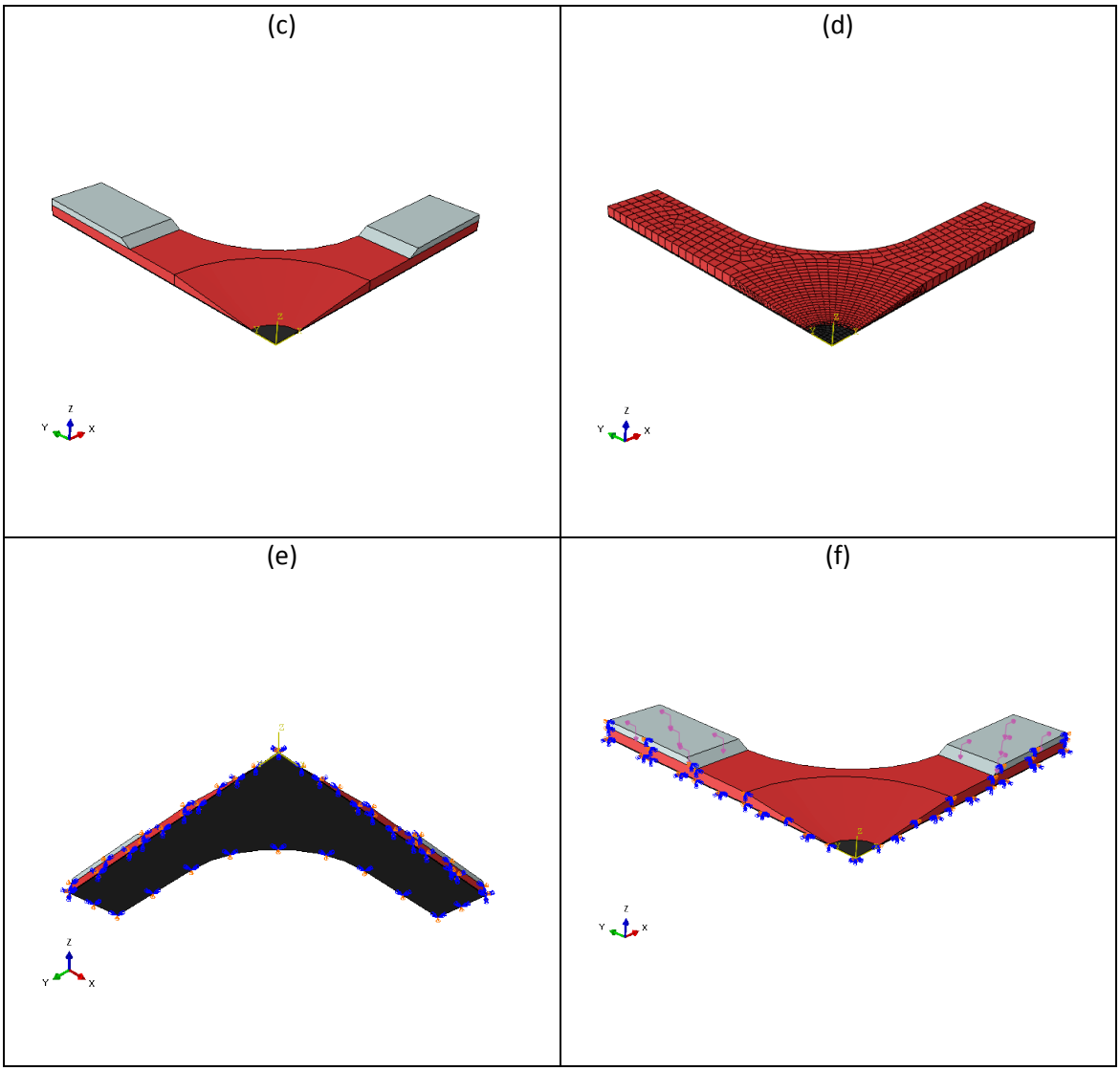

Figure 9. The specimen FE model full geometry ((a) and (b)); 1/8 of the whole geometry (c) and FEM mesh without the steel grips blocks on the arms (d); the boundary conditions in the X, Y and Z symmetry planes (e) and loading applied on the steel grips blocks (f).

For the 1/8 specimen model the total number of elements for the laminate part is 2076 (2040 quadratic hexahedral elements of type C3D20R and 36 quadratic wedge elements of type C3D15). Note that in this 1/8 specimen model only half the laminate thickness is considered, i.e. only 0.56mm thick, and only 1 layer of quadratic hexahedral/wedge elements is used through the thickness. The total number of elements for the large GFRP tab is 1419 (1 layer with 285 quadratic hexahedral elements of type C3D20R in the cruciform arms and about 2 layers with 1134 quadratic wedge elements of type C3D15 in the central circular conical section). The total number of elements for the steel grips block part is 44 (1 layer with 44 quadratic hexahedral elements of type C3D20R).

Modelling the central stress state in the biaxial tests

From the results of the simulations with the global specimen FE model for the various biaxial load conditions, the relation between the arm loads and the biaxial stress state in the central test section can be derived (Figure 10). It should be noted that these are only the homogenised stress values, averaged over the plies in the laminate. The global specimen FE model is used to first evaluate the elastic response of the specimen to the maximum single arm loading in 1-direction (F_1=200kN; F_2=0) by linear static analysis.

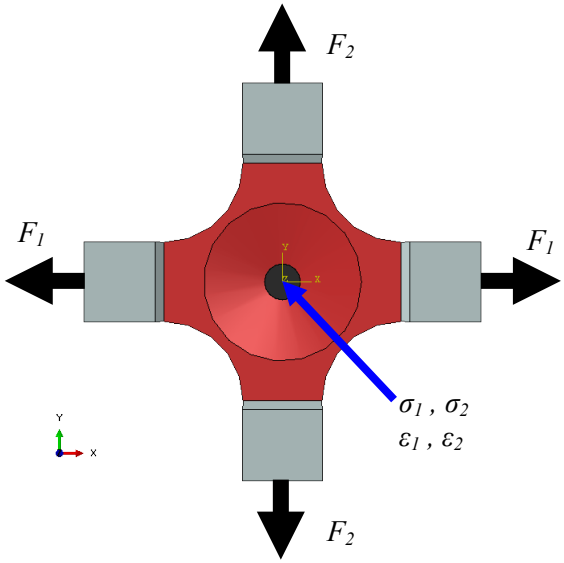

Figure 10. Illustration of the biaxial arm loads F_1 and F_2 as applied in the FEM analyses, and stresses and strains (σ_1,σ_2 and ε_1,ε_2) as evaluated in the centre point of the test section.

The resulting stress distribution in the specimen is shown in the Figure 11. The σ_1 and σ_2 stresses in the central test section represent the stress values averaged over the laminate plies. Their in-plane distributions are rather homogeneous within the central test section, with an envelope of stress values of about ±5% around the mean.

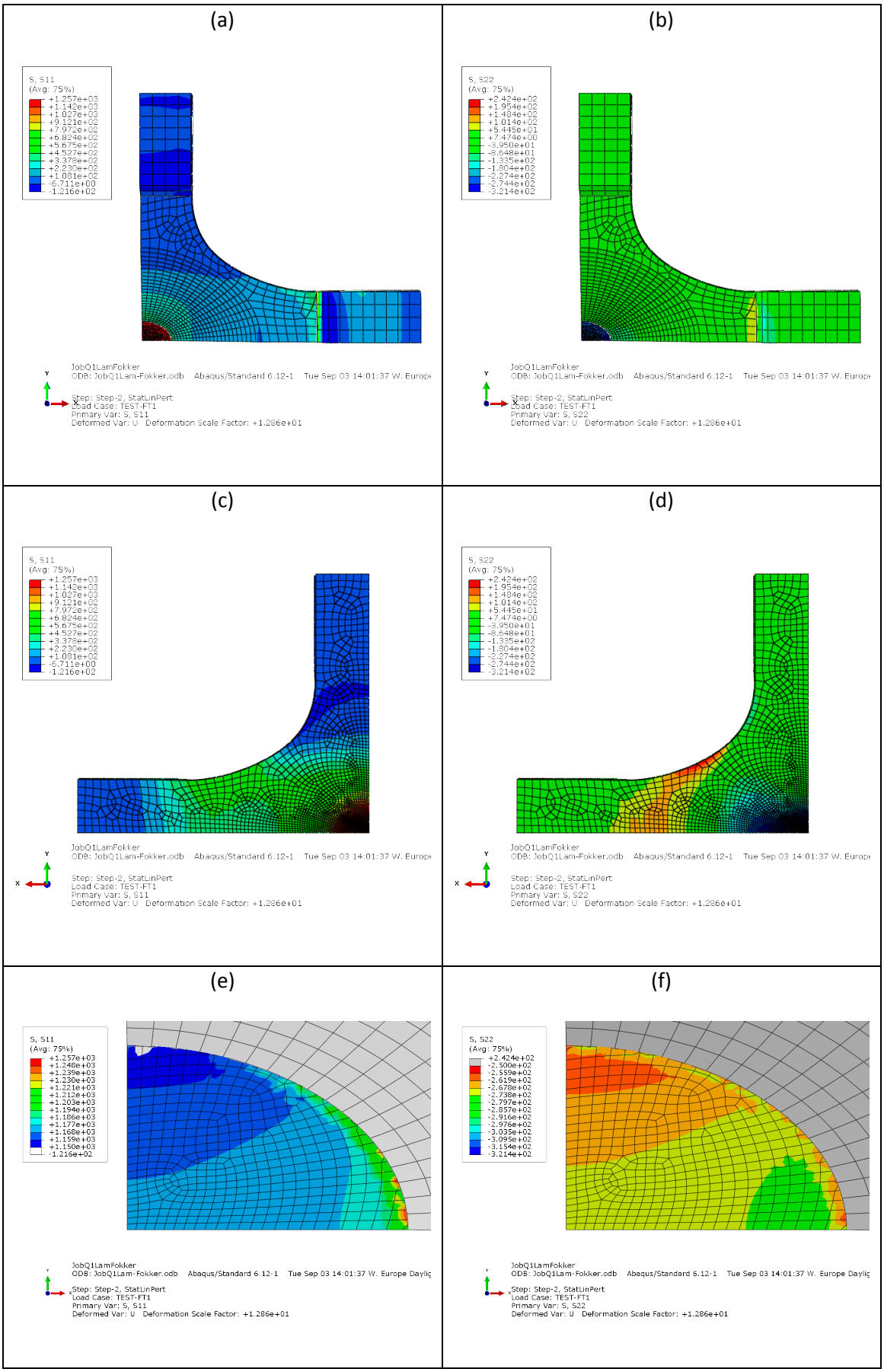

Figure 11. The resulting stress distributions in the specimen due to the maximum single arm loading in 1-direction (F_1=200kN; F_2=0). (a): σ_1 in upper surface of the specimen; (b): σ_2 in upper surface of the specimen; (c): σ_1 in mid-plane of

the specimen; (d): σ_2 in mid-plane of the specimen; (e): σ_1 in central test section of the specimen; (f): σ_2 in central test section of the specimen. For completeness, also the FEM mesh density is included in the graphs (note: quadratic elements).

The stress values for this load case in the centre point of the specimen are (approximately):

F_1=200kN; F_2=0: σ_1=1169MPa ; σ_2=-269MPa

Because of the symmetry of the global specimen FE model , it can be expected that the elastic response of the specimen to the maximum single arm compression loading in 2-direction (F_1=0 ; F_2=-200kN) would be vice versa, and the stress values in the centre point of the specimen would be (approximately):

F_1=0 ; F_2=-200kN: σ_1=269MPa ; σ_2=-1169MPa

This is indeed confirmed by the FEM analysis results, where these values are also found in the centre point of the specimen, see Figure 12. Moreover, the stress distributions in the specimen are also as expected from the symmetry of the load state.

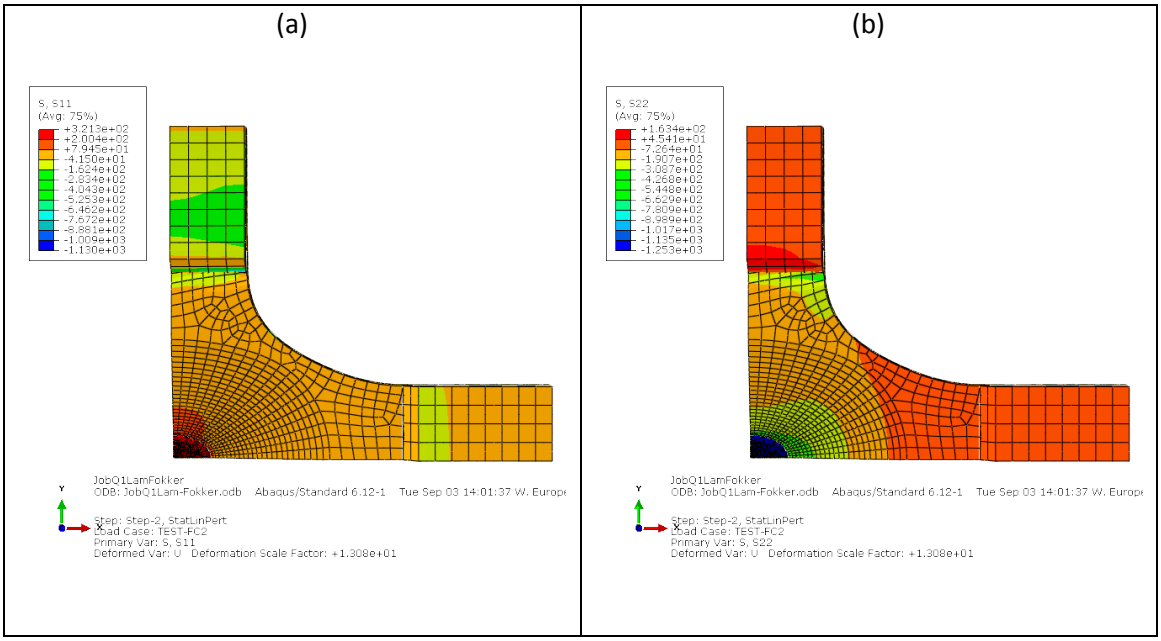

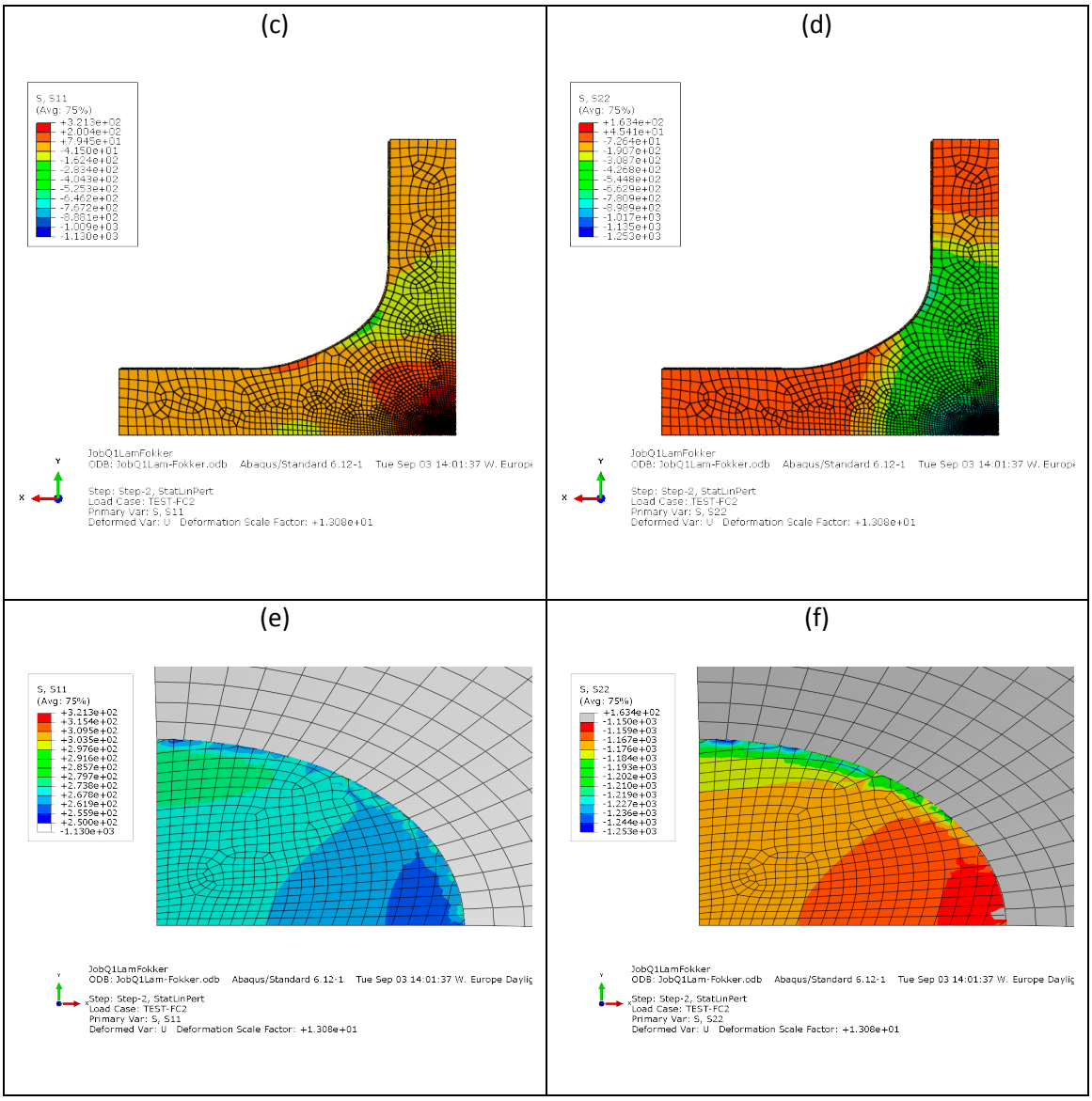

Figure 12. The resulting stress distributions in the specimen due to the maximum single arm compression loading in 2-direction (F_1=0 ; F_2=-200kN). (a): σ_1 in upper surface of the specimen; (b): σ_2 in upper surface of the specimen; (c): σ_1 in mid-plane of the specimen; (d): σ_2 in mid-plane of the specimen; (e): σ_1 in central test section of the specimen; (f): σ_2 in central test section of the specimen.

This linear FE model can be used to easily predict the stress and strain state in the specimen. Because the relation between the arm loads and the central stress and strain values in the specimen is of particular interest in this study, a simple algebraic model is derived for this relation from the linear FE results. Therefore, first the relations between the stresses in the centre point of the specimen and the arm loads in 1 and 2 directions (corresponding to the laminate 0^o and 90^o directions, respectively) are expressed as a general linear relationship:

$$\sigma_1 = \alpha_{10} + \alpha_{11}F_1 + \alpha_{12}F_2 \quad (1)$$

$$\sigma_2 = \alpha_{20} + \alpha_{21}F_1 + \alpha_{22}F_2 \quad (2)$$

The unknown coefficients α_{ij} can now be determined from the stress values found from the FEM analyses. The stress is zero in the un-loaded state, this yields: $\alpha_{10} = \alpha_{20} = 0$. Moreover, because of the symmetry of the stress state (as shown with the FE results above) it is found:

$\alpha_1 := \alpha_{11} = \alpha_{22}$; $\alpha_2 := \alpha_{12} = \alpha_{21}$, and with this the stress relation can be simplified to:

$$\sigma_1 = \alpha_1 F_1 + \alpha_2 F_2 \quad (3)$$

$$\sigma_2 = \alpha_2 F_1 + \alpha_1 F_2 \quad (4)$$

Solving the unknown coefficients for (F_1=200kN; F_2=0; σ_1=1169MPa ; σ_2=-269MPa) yields:

$$\alpha_1 = \frac{1169\text{MPa}}{200\text{kN}} = 5.845\frac{\text{MPa}}{\text{kN}} \quad ; \quad \alpha_2 = \frac{-269\text{MPa}}{200\text{kN}} = -1.345\frac{\text{MPa}}{\text{kN}} \quad (5)$$

Now the aim is to express the biaxial stress state in terms of the biaxial arm loads. For convenience of notation, the following ratios between the linear biaxial coefficients, the biaxial arm loads and the biaxial stresses are introduced:

$$\alpha = \frac{\alpha_1}{\alpha_2} = \frac{5.845}{-1.345} = -4.346 \quad (6)$$

$$\beta = \frac{F_1}{F_2} \quad (7)$$

$$\gamma = \frac{\sigma_1}{\sigma_2} \quad (8)$$

And the linear biaxial stress equations are re-written:

$$\gamma = \frac{\sigma_1}{\sigma_2} = \frac{\alpha_1 F_1 + \alpha_2 F_2}{\alpha_2 F_1 + \alpha_1 F_2} = \frac{\alpha\alpha_2\beta F_2 + \alpha_2 F_2}{\alpha_2\beta F_2 + \alpha\alpha_2 F_2} = \frac{\alpha\beta + 1}{\beta + \alpha} \quad (9)$$

Note that α is a constant that depends on the geometry and material properties of the specimen (and on the boundary conditions applied in the biaxial tests); note that β is just the ratio between the 1 and 2 direction arm loads in any given biaxial load state.

With this simple algebraic model for the biaxial stress ratio (γ), the arm loads ratio (β) that is needed to achieve a desired biaxial stress ratio in the specimen centre can be simply determined. For example, the biaxial stress ratio $\gamma = 0$ (i.e. σ_1=0 ; σ_2≠0) is achieved by the arm loads ratio:

$$\alpha\beta + 1 = 0 \quad \Rightarrow \quad \beta = -\frac{1}{\alpha} = 0.23 \tag{10}$$

And the biaxial stress ratio $\gamma = \infty$ (i.e. σ_2=0 ; σ_1≠0) is achieved by the arm loads ratio:

$$\beta + \alpha = 0 \quad \Rightarrow \quad \beta = -\alpha = 4.346 \tag{11}$$

Alternatively, if the arm loads ratio $\beta = 0$ (i.e. F_1=0 ; F_2≠0) then the biaxial stress ratio γ is:

$$\gamma = \frac{1}{\alpha} = -0.23 \tag{12}$$

Or if the arm loads ratio $\beta = \infty$ (i.e. F_2=0 ; F_1≠0) then the biaxial stress ratio γ is:

$$\gamma = \lim_{\beta \to \infty} \frac{\alpha\beta + 1}{\beta + \alpha} = \alpha = -4.346 \tag{13}$$

With these ratios the required arm loads for the intended biaxial tests can be determined.

Modelling the central strain state in the biaxial tests

From the linear static FE model evaluation of the elastic response of the cruciform specimen to the maximum single arm loading in 1-direction (F_1=200kN; F_2=0) also the resulting strain distributions in the specimen are found, as shown in the Figure 13.

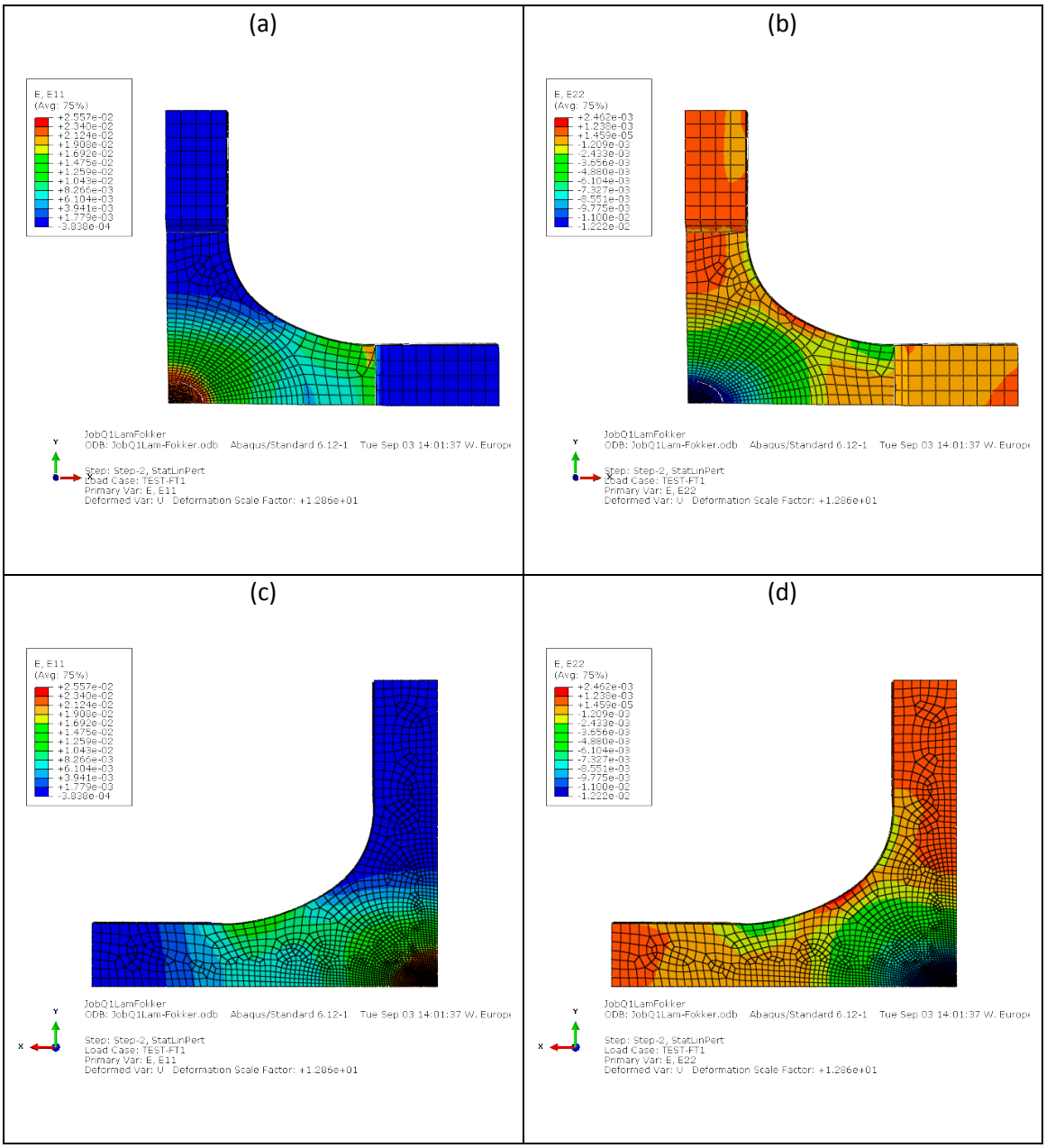

Figure 13. The resulting strain distributions in the specimen due to the maximum single arm loading in 1-direction (F_1=200kN; F_2=0). (a): ε_1 in upper surface of the specimen; (b): ε_2 in upper surface of the specimen; (c): ε_1 in mid-plane of the specimen; (d): ε_2 in mid-plane of the specimen.

The strain values for this load case in the centre point of the specimen are (approximately):

F_1=200kN; F_2=0: ε_1=0.0232 ; ε_2=-0.0117

Because of the symmetry of the specimen (geometry and layup) and the loading, the elastic response of the specimen to the maximum single arm compression loading in y-direction (F_1=0 ; F_2=-200kN) are vice versa, as expected, and the strain values in the centre point of the specimen are therefore (approximately):

F_1=0 ; F_2=-200kN: ε_1=0.0117 ; ε_2=-0.0232

Indeed this result is confirmed from the FEM analysis.

With the simple algebraic model for the biaxial stress state and the arm loads and considering linear orthotropic material behaviour of the laminate, also the relations between the arm loads and the biaxial strain state in the central test section can be derived. Assuming plane stress conditions in the central test section of the laminate, the in-plane stress-strain relation is expressed as:

$$\begin{bmatrix} \varepsilon_1 \\ \varepsilon_2 \\ 2\varepsilon_{12} \end{bmatrix} = \begin{bmatrix} \frac{1}{E_1} & -\frac{\nu_{21}}{E_2} & 0 \\ -\frac{\nu_{12}}{E_1} & \frac{1}{E_2} & 0 \\ 0 & 0 & \frac{1}{G_{12}} \end{bmatrix} \begin{bmatrix} \sigma_1 \\ \sigma_2 \\ \sigma_{12} \end{bmatrix} \tag{14}$$

Using the in-plane effective stiffness properties of the laminate (**Error! Reference source not found.**):

$$\begin{aligned} &\nu_{12} = \nu_{21} = \nu = 0.31 \\ &E_1 = E_{11} = E_2 = E_{22} = E = 54.0GPa \\ &G_{12} = G = 20.6GPa \end{aligned} \tag{15}$$

It is found:

$$\begin{aligned} \varepsilon_1 &= \frac{1}{E}[\sigma_1 - \nu\sigma_2] \\ \varepsilon_2 &= \frac{1}{E}[\sigma_2 - \nu\sigma_1] \\ \varepsilon_{12} &= \frac{1}{2G}\sigma_{12} \end{aligned} \tag{16}$$

Consequently, for the biaxial strain ratio in the central test section of the laminate it can be found:

$$\delta = \frac{\varepsilon_1}{\varepsilon_2} = \frac{\sigma_1 - \nu\sigma_2}{\sigma_2 - \nu\sigma_1} = \frac{\gamma\sigma_2 - \nu\sigma_2}{\sigma_2 - \nu\gamma\sigma_2} = \frac{\gamma - \nu}{1 - \nu\gamma} \tag{17}$$

This can also be expressed in the biaxial constant α and the biaxial arm loads ratio β:

$$\delta = \frac{\varepsilon_1}{\varepsilon_2} = \frac{\frac{\alpha\beta+1}{\alpha+\beta} - \nu}{1 - \nu\frac{\alpha\beta+1}{\alpha+\beta}} = \frac{1+\alpha\beta-\nu(\alpha+\beta)}{\alpha+\beta-\nu(\alpha\beta+1)} \quad (18)$$

A linear relationship between the biaxial strains and arm loads similar to the biaxial stresses can be expressed:

$$\varepsilon_1 = \chi_1 F_1 + \chi_2 F_2 \quad (19)$$

$$\varepsilon_2 = \chi_2 F_1 + \chi_1 F_2 \quad (20)$$

Solving the unknown coefficients $\chi_{1,2}$ for the single arm load case (F_1=200kN; F_2=0; ε_1=0.0232 ; ε_2=-0.0117) yields:

$$\chi_1 = \frac{0.0232}{200\text{kN}} = 116.0e-6\frac{1}{\text{kN}} \quad (21)$$

$$\chi_2 = \frac{-0.0117}{200\text{kN}} = -58.5e-6\frac{1}{\text{kN}} \quad (22)$$

Overview of the central stress and strain state in the intended biaxial tests

Tests in the following biaxial conditions are intended (Table 3), where the tests are expressed in biaxial tension and compression components.

Table 3. Explanation and coding of the intended biaxial test conditions.

Biaxial test code	Description	Expected stress/strain in gauge section
T1	uni-axial tension validation test in 1-direction	σ_1>0 ; σ_2=~0 ; ε_1>0 ; ε_2<0
C2	uni-axial compression validation test in 2-direction	σ_2<0 ; σ_1=~0 ; ε_1>0 ; ε_2<0
T1/T2	bi-axial tension/tension test	σ_1=σ_2>0; ε_1>0 ; ε_2>0
2T1/T2	bi-axial tension/tension test	σ_1= 2*σ_2 >0; ε_1>0 ; ε_2>0
T1/C2	bi-axial tension/compression test	σ_1= -σ_2 >0; ε_1>0 ; ε_2<0
C1/C2	bi-axial compression/compression test	σ_1=σ_2<0; ε_1<0; ε_2<0

With the biaxial stress-, strain- and load-ratios, the required arm loads for the intended biaxial tests can be determined, as given in the Table 4. For completeness also the additional load cases (FT1, FC2 and F2T1/T2) are given, representing the single, and combined, arm loads in 1- and 2-direction (i.e. F_1>0 and F_2=0; F_1=0 and F_2<0; F_1=2F_2 and F_2>0).

Table 4: Overview of the intended biaxial tests (T1,...,C1/C2) and additional load cases (FT1, FC2, F2T1/T2), with the values of the intended biaxial stress ratios and of the required arm load ratios for the cruciform specimen.

Test ID	Stresses in test-section	Stress ratio	Strains in test-section	Strain ratio	Arm forces	Arm force ratio
T1	σ_1>0 σ_2=0	$\gamma = \infty$	ε_1>0 ε_2=ε_1/-3.2	$\delta = \frac{1}{-\nu}$ $= -3.2$	F_1>0 F_2=F_1/β	$\beta = -\alpha$ $= 4.346$
C2	σ_1=0 σ_2<0	$\gamma = 0$	ε_1=-0.31ε_2 ε_2<0	$\delta = -\nu$ $= -0.31$	F_1= βF_2 F_2<0	$\beta = -\frac{1}{\alpha}$ $= 0.23$
T1/T2	σ_1>0 σ_2=σ_1	$\gamma = 1$	ε_1>0 ε_2=ε_1	$\delta = 1$	F_1>0 F_2=F_1	$\beta = 1$
2T1/T2	σ_1>0 σ_2=σ_1/2	$\gamma = 2$	ε_1>0 ε_2=ε_1/ 4.45	$\delta = \frac{2-\nu}{1-2\nu}$ $= 4.45$	F_1>0 F_2=F_1/β	$\beta = \frac{1-2\alpha}{2-\alpha}$ $= 1.527$
T1/C2	σ_1>0 σ_2=-σ_1	$\gamma = -1$	ε_1>0 $\varepsilon_1/\varepsilon_2$=-1	$\delta = -1$	F_1>0 F_2=-F_1	$\beta = -1$
C1/C2	σ_1<0 σ_2=σ_1	$\gamma = 1$	ε_1<0 ε_2=ε_1	$\delta = 1$	F_1<0 F_2=F_1	$\beta = 1$
Additional loadcases	**Stresses in test-section**	**Stress ratio**	**Strains in test-section**	**Strain ratio**	**Arm forces**	**Arm force ratio**
FT1	σ_1>0 σ_2=σ_1/-4.346	$\gamma = \alpha$ $= -4.346$	ε_1>0 ε_2=ε_1/-1.98	$\delta = \frac{\alpha-\nu}{1-\alpha\nu}$ $= -1.98$	F_1>0 F_2=0	$\beta = \infty$
FC2	σ_1=-0.23σ_2 σ_2<0	$\gamma = \frac{1}{\alpha}$ $= -0.23$	ε_1=-0.5ε_2 ε_2>0	$\delta = \frac{1/\alpha-\nu}{1-\nu/\alpha}$ $= -0.5$	F_1=0 F_2<0	$\beta = 0$

F2T1/T2	$\sigma_1>0$ σ_1/σ_2=3.28	$\gamma = \frac{2\alpha+1}{2+\alpha} = 3.28$	$\varepsilon_1>0$ $\varepsilon_2=\varepsilon_1$/-180.8	$\delta = \frac{1+2\alpha-\nu(2+\alpha)}{2+\alpha-\nu(2\alpha+1)} = -180.8$	$F_1>0$ $F_2=F_1/2$	$\beta = 2$

Checking strains in global FE model

To investigate more specifically the ply-by-ply effects in the laminate of the central test section, a more detailed FE model of the specimen is considered. This model contains the full 3D linear elastic orthotropic representation of each individual ply of the laminate, accounting explicitly for the orientations and properties per ply as given in Table 1 for in-plane; the plies' out-of-plane properties (E_{33}, G_{23}, G_{13} , v_{23}, v_{13}) are adopted from Table 2. Because of the ±45° plies that are included in this model as 3D layers in the laminate, the in-plane symmetry of the specimen cannot be used to simplify the model. Therefore the upper half-specimen model is considered with symmetry boundary conditions (Z-displacement is 0) in the symmetry plane (Z=0). For this half-specimen model the total number of elements for the laminate is 16644 quadratic hexahedral elements of type C3D20R. Note that in this half-specimen model only half the laminate thickness is considered, i.e. containing 4 plies each 0.14mm thick, and each ply contains 1 layer of 4161 quadratic hexahedral elements.

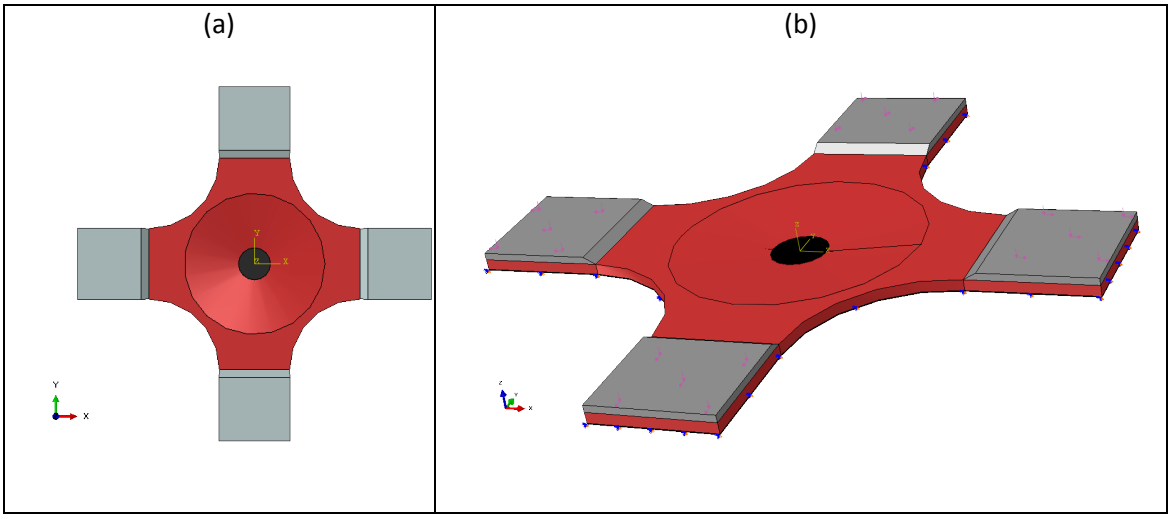

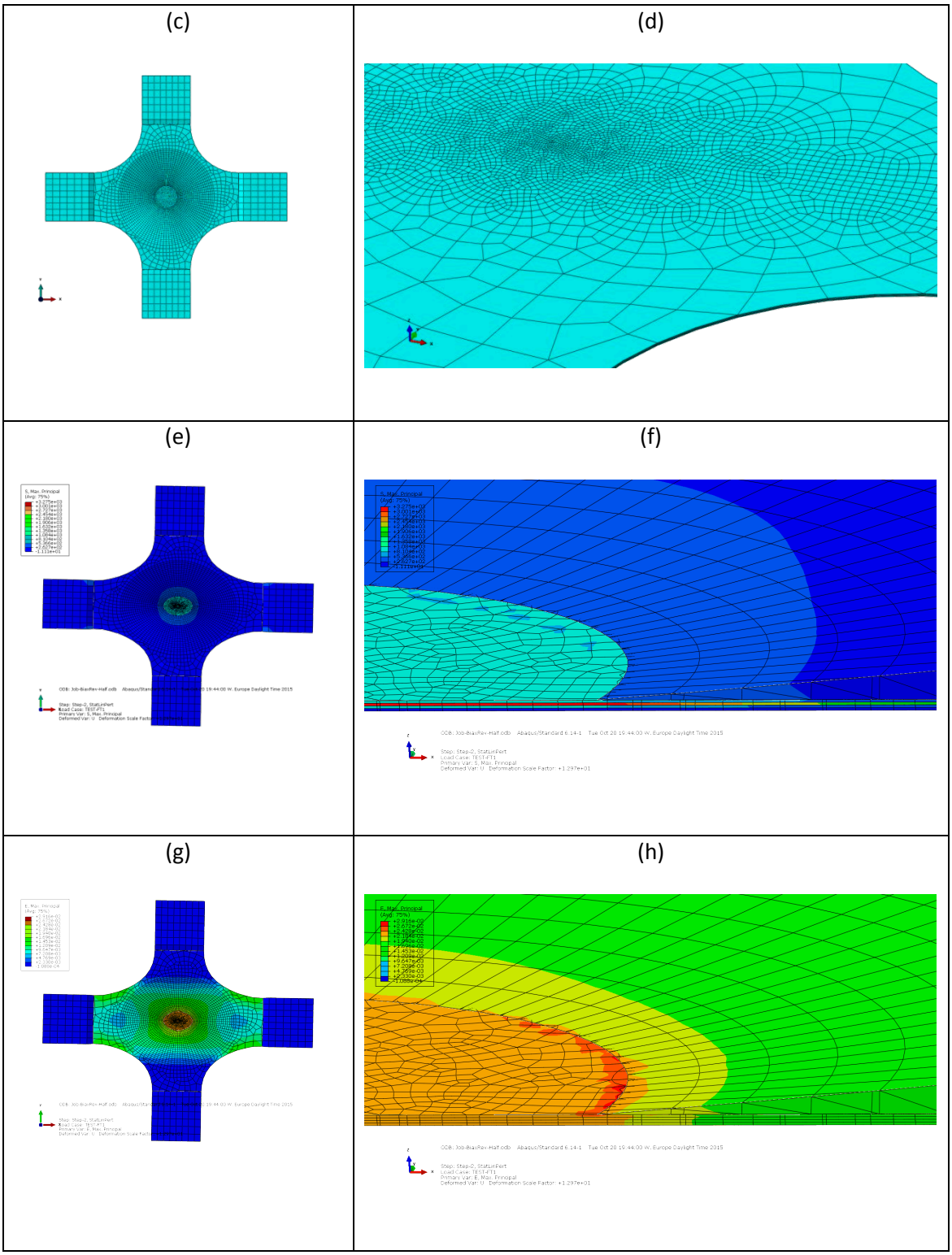

Figure 14. Top view of the specimen FE model full geometry (a) and the upper half-specimen model with loads and boundary conditions in the Z symmetry plane (b). Top view of the mesh of the half-specimen model (c) and zoom-in on the mesh of the 4 plies of the upper half of the laminate part (d). For the FT1 load case the maximum principal stress σ_{pm} is given in the upper surface of the half specimen FE model (e) and in each of the 4 plies in a cross-section in the gauge area (f). Similarly for the FT1 load case the maximum principal strain ε_{pm} is given in the upper surface of the half specimen FE model (e) and in each of the 4 plies in a cross-section in the gauge area (f).

With this detailed FE model of the half-specimen also linear FE analyses of each of the intended biaxial test conditions is performed and the resulting stresses and strains are evaluated. As expected,

the stress values differ significantly over the plies (i.e. through the thickness), as illustrated by the principal stress plots for the FT1 load case in Figure 14. The strain values, as expected, are rather homogeneous in the whole gauge area and more or less equal over the plies (i.e. through the thickness), as illustrated by the principal strain plots for the FT1 load case in Figure 14.

The resulting strains are also compared to the strain values from the 1/8 specimen FE model. Similar strain values are found in these two models, as illustrated by the strain plots for the FT1 load case in Figure 15. Such good correspondence between the strain values from the 1/8 specimen and the half-specimen FE models is also found for in the other load cases. Therefore it is concluded that the averaged stress and strain values found with the 1/8 specimen FE model are reasonably accurate.

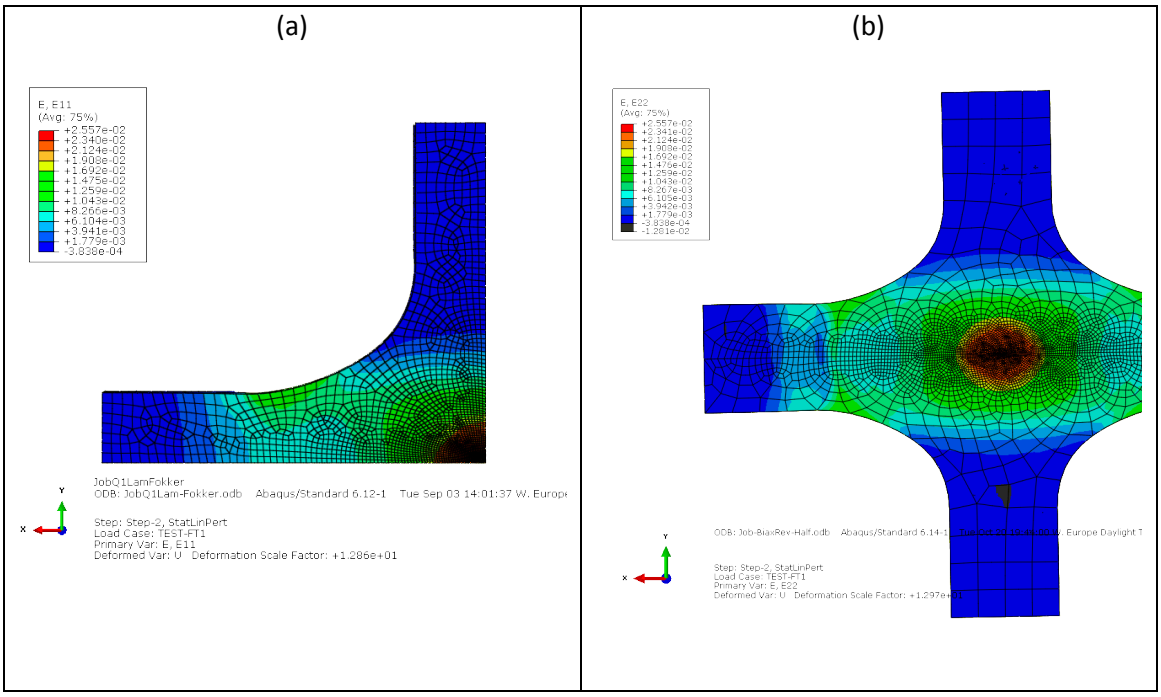

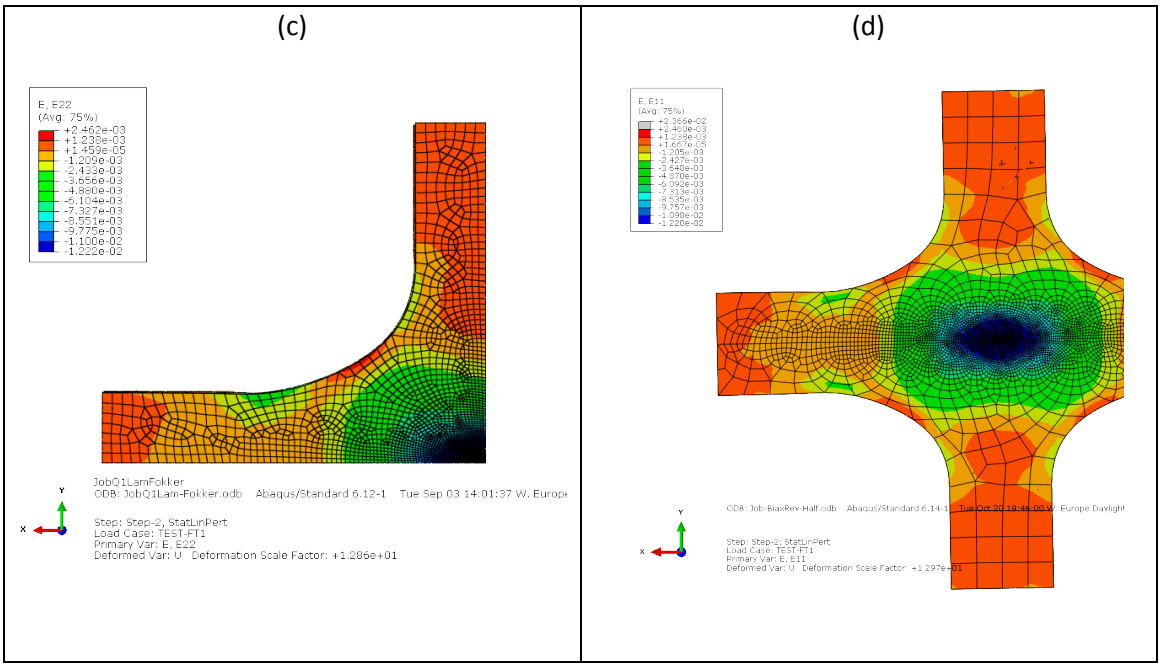

Figure 15. Comparison of the resulting mid-ply strain distributions in the 1/8-specimen (on the left) and the half-specimen (on the right) FE models for the FT1 load case (maximum single arm loading in 1-direction F_1=200kN; F_2=0). Note that in the half-specimen model the ε_1 strain is in the local fibre direction, i.e. in the global Y direction because the mid-ply has a 90° fibre orientation. (a): ε_1 in mid-plane of the 1/8 specimen FE model; (b): ε_2 in mid-plane (90° ply!) of the half specimen FE model; (c): ε_2 in mid-plane of the 1/8 specimen FE model; (d): ε_1 in mid-plane (90° ply!) of the half specimen FE model. Similar good corresponding strain values are also found for the other load cases.

Biaxial tests and results

Test plan

The cruciform specimens are used for the actual assessment of the failure behaviour of the CFRP laminate under in-plane biaxial loading at various biaxial load ratios. Because of the QI properties of the laminate, the tests are limited to one half of the biaxial strain plane (see Figure 16).

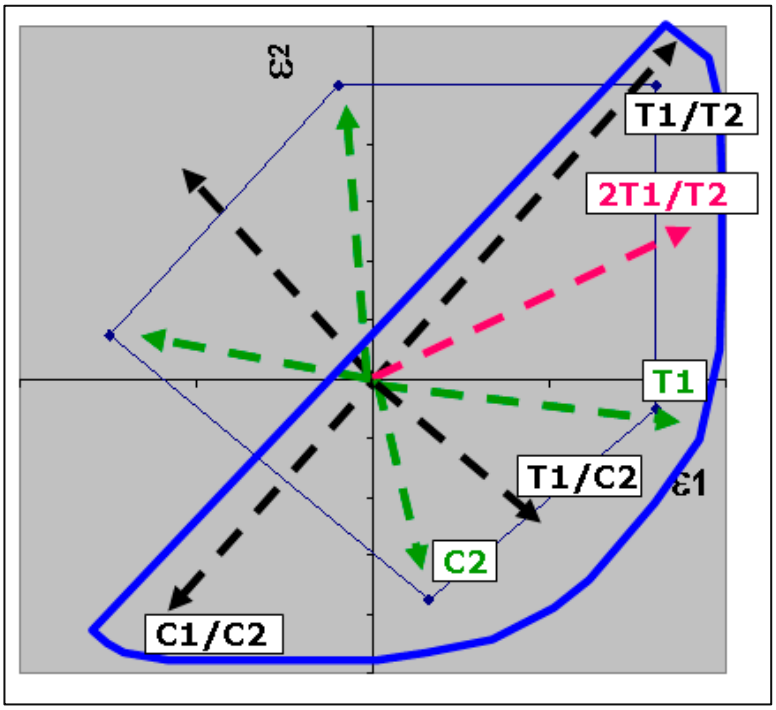

Figure 16 The intended biaxial tests on the QI laminate, illustrated in the biaxial strain plane (ε_1,ε_2). Because of the QI properties of the laminate, the tests are limited to one half of the biaxial strain plane.

All tests are performed with cruciform specimens with a plain (un-notched) test section and with an open-hole test section. All tests are performed only with “non-exposed” specimens in the “as-received” state, at Room Temperature Ambient (RTA) conditions.

The biaxial tests are executed with the measurements according to the test schedule in the Table 5. The strain gauges were applied only on the specimens 1-4. High-speed (HS) camera recordings were made only on the specimens 1-4, 7 and 24. Aramis DIC measurements of the central test section (“Aramis zoom”) were made with stereoscopic cameras (“3D”) on all the specimens (Table 5).

Table 5. The overview of all the biaxial tests and measurements that are recorded in each test.

Specimen no.	Test type	Strain gauges	HS camera	Aramis overview	Aramis zoom	Plain/OH
1	T1	Y	Y	3D	3D	plain
2	2T1/T2	Y	Y	3D	3D	plain
3	T1/T2	Y	Y	N	3D	plain
4	T1/C2	Y	Y	N	3D	plain
5	C1C2	N	N	N	3D	plain
6	T1/T2	N	N	N	3D	plain
7	2T1/T2	N	Y	3D	3D	plain
8	2T1/T2-OH	N	N	N	3D	open hole
9	C1C2-OH	N	N	N	3D	open hole
10	T1/C2	N	N	N	3D	plain
11	C1/C2	N	N	N	3D	plain
12	C1/C2	N	N	N	3D	plain
13	C1C2	N	N	N	3D	plain
14	C1/C2-OH	N	N	N	3D	open hole
15	C1/C2-OH	N	N	N	3D	open hole
16	T1/C2-OH	N	N	N	3D	open hole
17	C2-OH	N	N	N	3D	open hole
18	2T1/T2-OH	N	N	N	3D	open hole
19	T1T2-OH	N	N	N	3D	open hole
20	T1/T2	N	N	N	3D	plain
21	2T1/T2	N	N	3D	2D	plain
22	T1C2	N	N	N	3D	plain
23	T1/T2-OH	N	N	N	3D	open hole
24	T1/T2-OH	N	Y	N	3D	open hole
25	T1-OH	N	N	N	3D	open hole
26	2T1/T2-OH	N	N	N	3D	open hole
27	T1/C2-OH	N	N	N	3D	open hole
28	T1/C2-OH	N	N	N	3D	open hole

Test measurements

The following quantities have been recorded during these biaxial tests:

1. horizontal specimen load (F_1) using the 2 load cells of the horizontal loading frame (Figure 5);
2. vertical specimen load (F_2) using the load cell of the MTS testing machine;
3. strains as measured in 0°, 90° and 45° directions (ε_1,ε_2,ε_{45}) with the central rosette strain gauge (only on 4 of the 28 specimens).[13]

These signals were recorded using an Autolog3000 data acquisition system manufactured by Peekel instruments.[21] Further the following measurements were made:

4. strain measurements with Aramis DIC system[12] on the test section surface at one side of the specimen;
5. high-speed camera video recordings[20] at one side of the specimen (opposite side as Aramis measurements; only on 6 of the 28 specimens).

Uni-axial conditions

From the 28 biaxial tests, only three tests are devoted to the evaluation of uni-axial load conditions in the specimen. The remaining 25 specimens have been devoted to the biaxial test conditions. It should be noted, that even when a uniaxial tension load in x-direction is applied to the specimen, a negative stress in y-direction develops due to transverse compression of the test section. Therefore biaxial arm loads shall be applied to achieve the uni-axial stress condition in the gauge section. The arm force ratio $\beta = -\alpha = 4.346$ is applied here, as explained earlier. Besides the uni-axial tension test of the un-notched specimen, also one uni-axial tension and one uni-axial compression test of notched specimens are performed.

Strain results

In this section the results from the strain measurements are evaluated. Load-strain curves for five different load cases (T1, 2T1/T2, T1/T2, T1/C2, C1/C2) are shown in Figure 17. The Aramis strains are obtained through an averaging procedure over an area of the specimen. Strain gauge results are included in the plots when available. Overall good agreement is found between the strain gauge data and the Aramis data.

(a): F_1 vs. ε_1 ; F_2=F_1/4.346

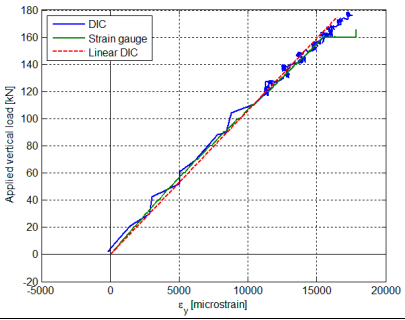

(b): F_1 vs. ε_2 ; F_2=F_1/4.346

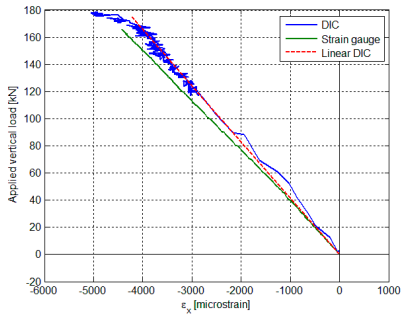

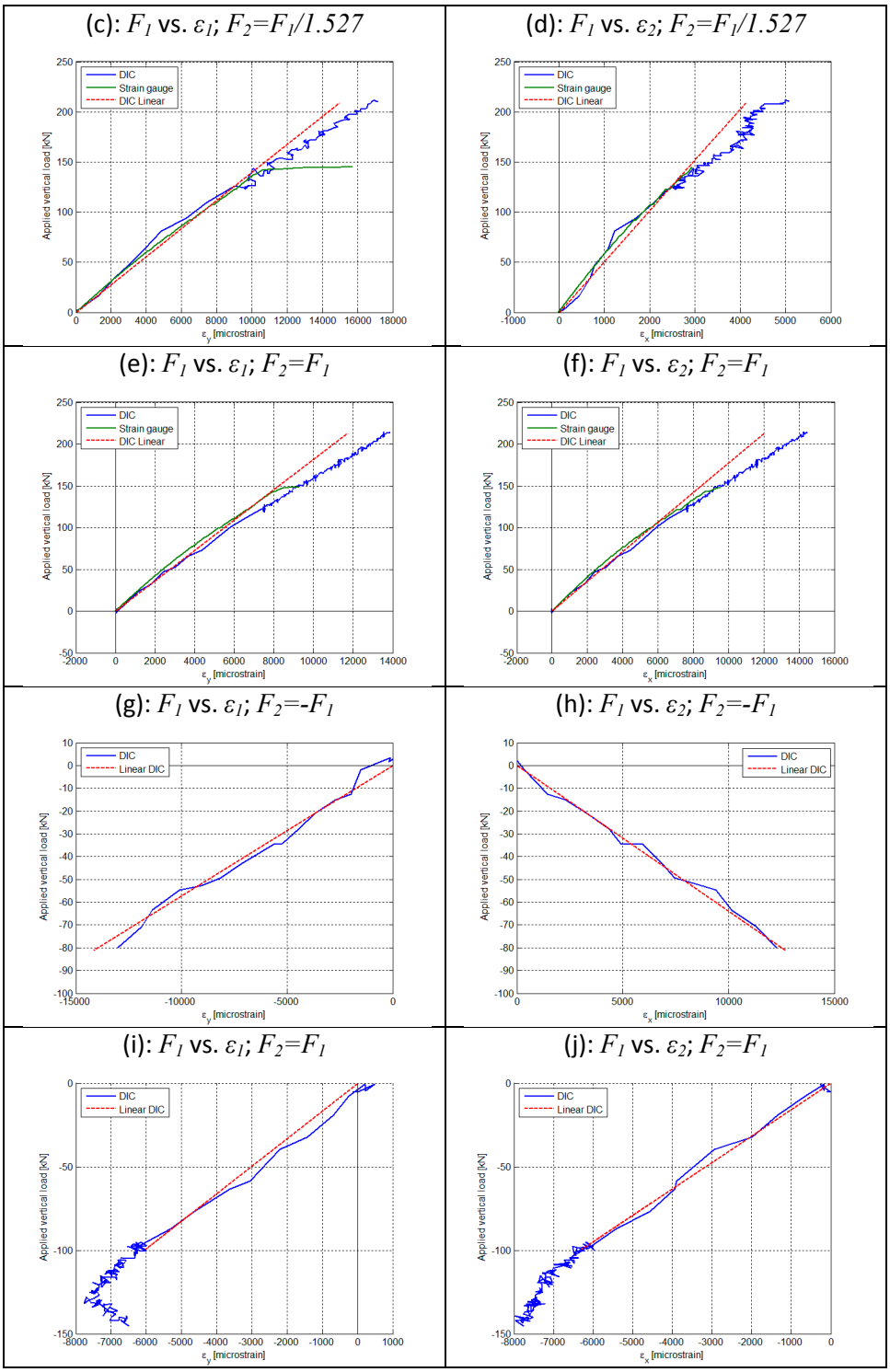

Figure 17. Load-strain curves for 5 different load cases. (a) and (b): T1 test; (c) and (d) : 2T1/T2 test; (e) and (f) : T1/T2 test ; (g) and (h): C1/T2 test (F_1 in compression; F_2 in tension); (i) and (j): C1/C2 test. Note that in all the graphs, F_1 corresponds to the vertical load in the test and ε_1,ε_2 correspond to ε_y,ε_x, resp.

As can be observed in the strain plots, the strain gauge data have only limited value because the strain gauge rosettes detach from the specimen far before final failure occurs due to the relatively high local strains in the test section. Moreover, the strain gauge measurements only yield the strain

in the centre of the test section whereas failure may be initiated in other locations. Therefore the Aramis strain measurements are used to determine the actual failure strain in the biaxial tests.

Failure strains and stresses

Failure strains ε_1 and ε_2 (in vertical and horizontal test rig axes, resp.) are derived in two different ways. The first method is to select a location on the linear regime of the load-strain relation and to scale this load and its corresponding strain to the Aramis measured failure load. This relation is shown by the dotted line in Figure 17. The failure stresses are calculated through the plane stress relations given below.

$$\sigma_1 = \frac{E}{1-\nu^2}(\varepsilon_1 + \nu\varepsilon_2) \tag{23}$$

$$\sigma_2 = \frac{E}{1-\nu^2}(\varepsilon_2 + \nu\varepsilon_1) \tag{24}$$

The second method is to directly read off the failure strains recorded by Aramis and to use the plane stress relations to compute the failure stresses. For each load case always one of the methods deemed to give the most realistic results. Hence, for the load cases T1, T1/C1 and C1/C2 the first method was used, while for the load cases T1/T2 and 2T1/T2 the second method has been used to compute the failure strain.

An overview of the failure loads and stresses from the biaxial tests is given in Table 6. Failure loads F_1 and F_2 are measured with the MTS test rig and the load cells[17]. Three specimens have invalid failure loads due to buckling or initial damage being present.

Table 6. Failure loads and stresses for different specimens.

Load case	Sp. no.	F_1 [kN]	F_2 [kN]	σ_1[MPa]	σ_2 [MPa]	Remark
T1	1	40	175	54	905	
T1-OH	25	22	95	28	491	
2T1/T2	2	137	209	621	1120	
2T1/T2-OH	26	76	116	-	-	
2T1/T2-OH	18	81	124	311	576	
T1/T2	3	213	213	1094	1119	

T1/T2-OH	23	130	130	619	627	
T1/T2-OH	24	122	122	-	-	
T1/C2	4	71	-71	-	-	Invalid, buckling
T1/C2	10	81	-81	494	-611	
T1/C2-OH	27	45	-45	277	-343	
T1/C2-OH	16	45	-45	-	-	
C1/C2	5	-146	-146	-714	-699	
C1/C2-OH	9	-90	-90	-440	-430	
C1/C2-OH	15	-73	-73	-	-	Invalid, damaged notch
C1/C2-OH	14	-76	-76	-	-	Invalid, damaged notch

Aramis strains interpretation

From the Aramis recordings the strain field is calculated and visualized by colour coding. Supplementary to the strain measurements described above, the visual recordings show the initiation of cracks, specific regions at which the strains reach excessive values or de-laminations through plotting the out-of-plane displacement. The Aramis visual recordings aid in determining at which applied load the specimen fails, such that together with the load-strain relations, a failure strain is obtained.

A typical Aramis recording is shown in Figure 18 in which the Von Mises strain recording prior to failure and after failure for a plain specimen under the load case biaxial tension (2T1/T2) is presented. A homogeneous strain field in the centre of the specimen is observed. The “red ring” does not represent high strain values but is an artefact from the Aramis strain calculation at the boundary of the test section due to the discontinuity in properties (laminate-tab surface). Figure 18(b) shows that failure of the specimen takes place in the centre and additionally, cracks occur in the tab. Figure 19 shows the applied vertical load plotted against the stage number. The stage represents an instance in time. The sudden decrease in load corresponds to the moment at which the specimen fails.

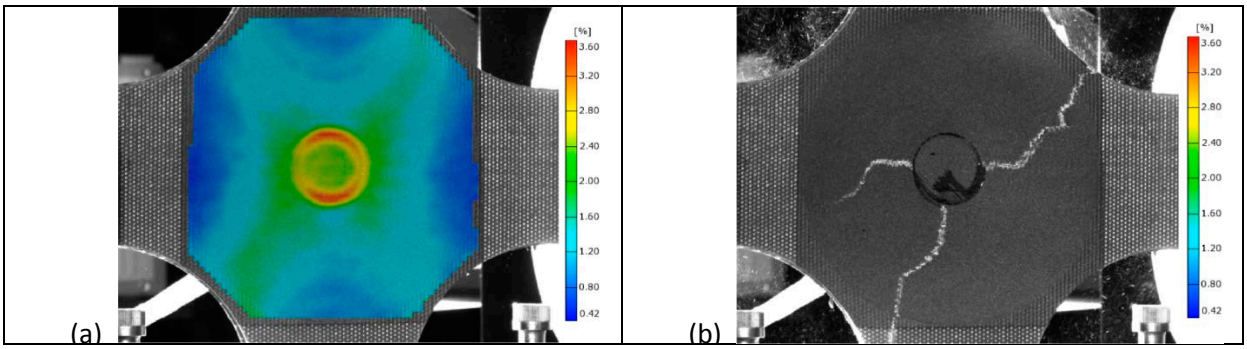

Figure 18. Aramis Von Mises strain for specimen 2 (2T1/T2): (a) just prior to failure, vertical load 210.4 kN; (b) After failure.

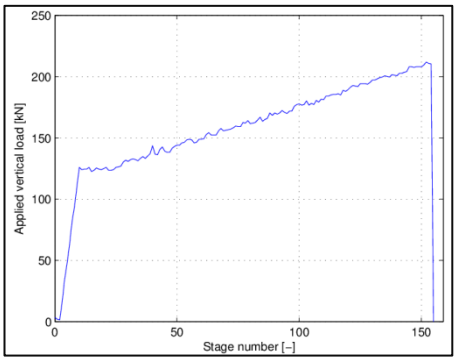

Figure 19. Applied vertical load versus stage number for specimen 2 (2T1/T2)

Specimen no. 23 and 24 are both subject to the T1/T2-OH load case. The difference in failure behaviour between the two specimens is shown in Figure 20. Both specimens show strain patterns in the direction of the fibres of the outer layer, i.e. in -45^{o} and +45^{o} directions for the specimen no. 23 and 24, respectively. These strain patterns probably correspond to resin rich areas and are observed more pronounced in specimen no. 23.

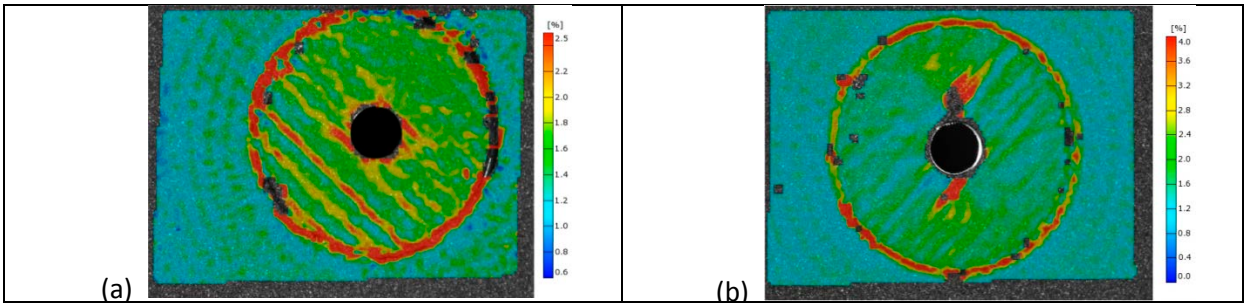

Figure 20. Aramis Von Mises strain with resin rich areas: (a) specimen 23 (T1/T2-OH); (b) specimen 24 (T1/T2-OH).

Specimen no. 9, 14 and 15 are all loaded in biaxial compression (C1/C2-OH). From detailed inspection of these open-hole specimens it was found that the latter two have damage due to drilling the notch, while specimen no. 9 does not have this. This is recognized in the performance and failure behaviour of these specimens. The failure loads of these initially damaged specimens (see Table 6) show significantly lower values (more than 14% difference) than for the un-damaged (specimen 9). The damage initiation and propagation among the three specimens differs due to this damage. The damage around the notch created an initial delamination in these specimens. As the load is increased the delamination expands around the notch. An example of this is shown in Figure 21 where for specimen no. 14 the out-of-plane displacement is shown. The displacement colour scale is set from -0.1 mm to 0.1 mm, which is approximately the ply thickness. Noteworthy is that the initial delamination is found to be at the location at which the damage due to drilling was induced. The delamination starts to propagate at a relatively low applied load. For the intact specimen a very minor out-of-plane displacement occurs at a relatively high load, just prior to failure, as is shown in Figure 22. Furthermore, the failure behaviour in the intact specimen is much more abrupt compared to the initially damaged specimens.

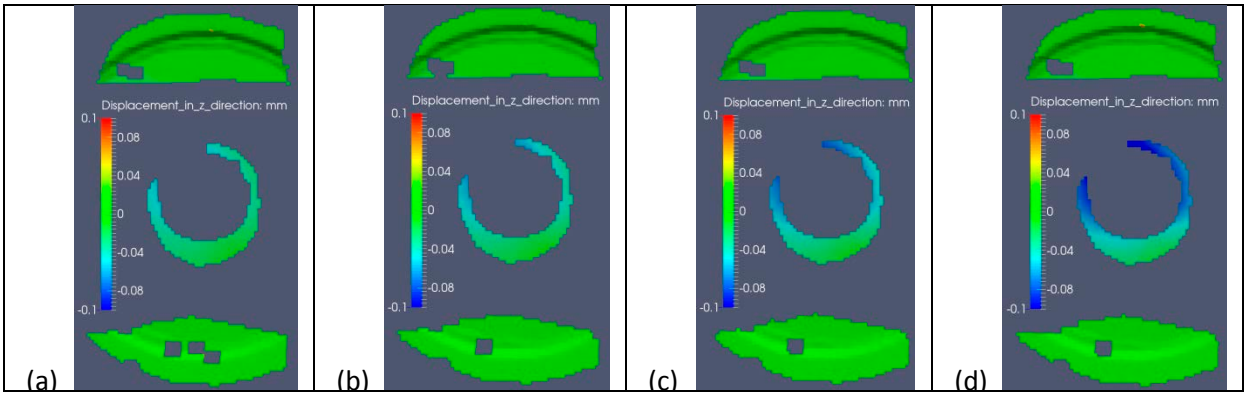

Figure 21. Out-of-plane displacement specimen 14 C1/C2-OH revealing de-laminations: (a) Vertical load -58.1kN; (b) -60.1 kN; (c) -72.8kN; (d) -74.kN.

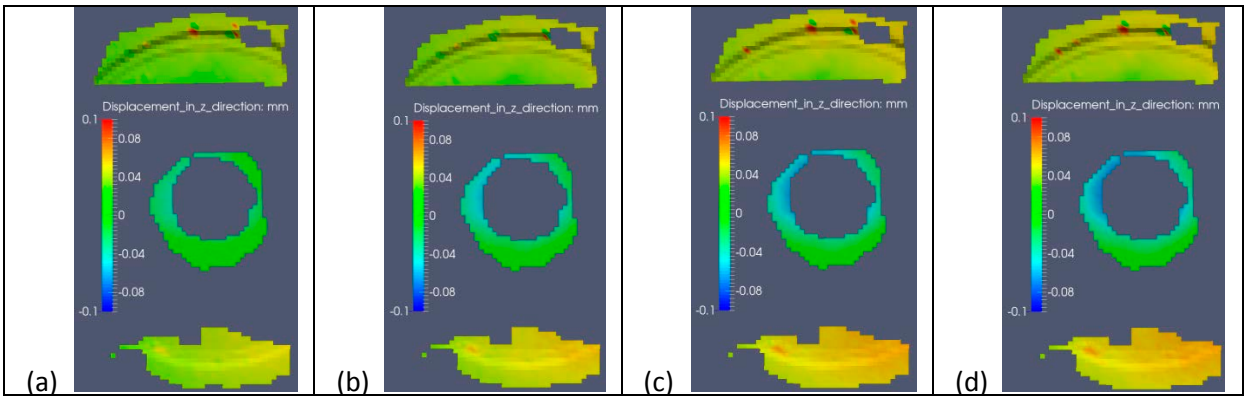

Figure 22. Out-of-plane displacement specimen 9 C1/C2-OH: (a) Vertical load -81.5kN; (b) -85.4kN; (c) -87.9kN; (d) -89.8 kN.

Biaxial failure Envelopes

Based on the observations from the Aramis recordings as well as the load-strain relations, a failure load and failure strain has been determined. From this the failure stresses have been computed for the different load cases. These failure stresses can be plotted to form a failure envelope, which represents the combinations of biaxial loading resulting in failure.

Figure 23 displays the failure envelopes for the plain specimens as well as for the open-hole specimens. The presented solid red data points are obtained through the above described procedure. With the generally used classical laminate theory the ply stress and strain for each ply in the laminate are determined. These stresses and strains are compared with the known allowable ply stresses and strains using the Puck failure criterion[27]. The input for the failure criterion are the properties as given in Table 1 and the recommended slope parameters ($p^t_{\perp}$=0.35; $p^c_{\perp}$=0.3; $p^t_{\perp\perp}$=0.25; $p^c_{\perp\perp}$=0.25) as given in[27]. Laminate failure occurs when the first ply exceeds the allowable fibre strength (f_1^t or f_1^c).

The theoretically predicted failure envelopes for both the plain specimen, based on the Puck failure criterion[27] and the open-hole specimen based on the stress-field method[22,23,24,25] in combination with the Whitney-Nuismer point stress method[26] are plotted. The two data points at the right-hand top in the plain specimen plot are directly based on Aramis strain recordings and the remaining data points

have been linearly scaled. The data points in the plot of the open-hole specimens have all been linearly scaled. Furthermore, in this same plot additional data points (black crosses) are given. These data points are based on observed damage initiation rather than actual failure and they show a closer correlation with the theoretically predicted envelope, as this envelope predicts first ply failure.

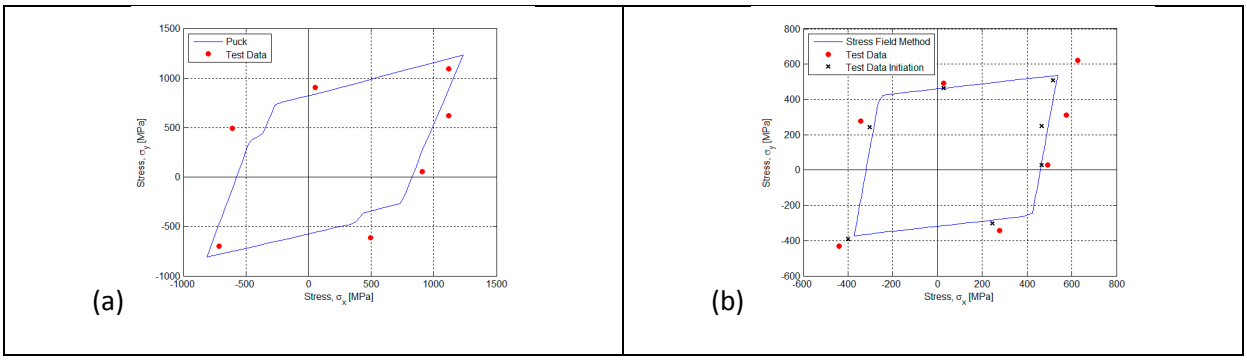

Figure 23. Failure envelopes: (a) plain specimens; (b) open-hole specimens.

Conclusions

The objective of the present study was to determine by experiments the biaxial failure data for laminates produced by Fokker based on the UD carbon reinforced thermoplastic material (AS4D/PEKK-FC). In particular the general validity of bi-axial failure criteria, which are mostly based on thermoset composite materials, has been checked for thermoplastic composite materials.

A biaxial test program covering various biaxial load combinations in tension-tension, tension-compression and compression-compression has been successfully executed and biaxial failure values have been determined.

It was found that the biaxial load-case with at least one compression components, buckling or bending of the laminate in the central test section of the specimen was very critical. Therefore an anti-buckling guide (ABG) was successfully designed and applied in the biaxial tension-compression and compression-compression load-cases. It appeared that the ABG should support an as large as possible area of the test section in order to be most effective. However, a small area of the test-

section had to remain unsupported by the ABG to allow for the DIC strain measurements with the Aramis DIC system.

Besides the experimental biaxial test program, also FE modelling and analyses are used, both to predict the global outcomes of the biaxial tests and to interpret the test results.

From the Aramis DIC system failure loads and strains have been obtained. Failure stresses have been determined by either scaling the failure load to the linear portion of the load-strain relations or by directly considering the failure strain recorded by Aramis. The stresses have been used to construct failure envelopes for the plain and open-hole specimens. For both envelopes it is concluded that good agreement is found between the theoretically predicted envelopes and the data from the tests. This confirms that the general failure criteria, primarily developed for thermoset material, are also valid for thermoplastic material and that thermoplastic specific properties do not adversely affect the current failure theories, nor that effects are missed in those criteria.

Based on the findings given in this report it is expected that composite parts with lower weight can be made as compared to parts that are designed with the previous uni-axially based failure criteria.

Acknowledgement

This work was supported by the Netherlands Enterprise Agency (http://www.rvo.nl), grant number SRP09015/59915N. The support of mr. R. Sieders, mr. B. van der Kolk and mr. H. Jongstra of NLR in the preparation and assembly of the cruciform specimens and in the design of the biaxial test rig is gratefully acknowledged.

References

1. Kassapoglou C. *Design and analysis of composite structures: with applications to aerospace structures*. Wiley, 2010.

2. National Materials Advisory Board, National Research Council (US). *The Place for Thermoplastic Composites in Structural Components: Report of the Committee on Thermoplastic Composites as Structural Components*. National Academies, 1987.
3. Hinton MJ, Kaddour AS and Soden PD. Failure criteria in fibre reinforced polymer composites: the world-wide failure exercise. *A composites science and technology compendium*. Elsevier, 2004.
4. Wang J, Callus PJ and Bannister MK. Experimental and Numerical Investigation of the Tension and Compression Strength of Un-notched and Notched Quasi-isotropic Laminates. *Composite Structures* 2004; 64(3-4): 297-306.
5. Orifici AC, Herszberg I and Thomson RS. Review of methodologies for composite material modelling incorporating failure. *Composite Structures* 2008; 86: 194-210.
6. Hannon A and Tiernan P. A review of planar biaxial tensile test systems for sheet metal. *J. Mat.Proc.Technol.* 2008; 198: 1-13.
7. Susuki I. Biaxial testing of composite laminates using cruciform specimens. In: *Proceedings of the 8th International Conference on Composite Materials (ICCM-8)*, Honolulu, USA, 1991.
8. Susuki I and Ishikawa H. (1991). Designing of cruciform specimen for strength evaluation of composite laminate. In: *Proceedings of the 2nd Japan International SAMPE Symposium and Exhibition (JISSE-2)*, Chiba, Japan, 1991.
9. Kumazawa H and Takatoya T. Biaxial strength investigation of CFRP composite laminates by using cruciform specimens. In: *Proceedings of the 17th International Conference on Composite Materials (ICCM-17)*, Edinburgh, UK, 2009.
10. Huang Y, Ha SK, Koyanagi J, Melo JDD, Kumazawa H and Susuki I. Effects of an open hole on the biaxial strengths of composite laminates. *Journal of Composite Materials* 2010; 44(20): 2429-2445.
11. Kureemun U, Ridha M and Tay TE. Biaxial tensile-compressive loading of unnotched and open-hole carbon epoxy crossply laminates. *Journal of Composite Materials* 2014; 0(0): 1–21.

12. GOM mbH, Germany. Aramis DIC system http://www.gom.com/metrology-systems/digital-image-correlation.html (accessed 3-7-2014).
13. Vishay Precision Group Inc., USA. http://www.vishaypg.com/micro-measurements (accessed 6-10-2014).
14. Charvat IMH and Garrett GG. The Development of a closed-loop, servo-hydraulic test system for direct stress monotonic and cyclic Crack propagation studies under biaxial loading. *Journal of Testing and Evaluation* 1980; 8(1): 9-18.
15. MTS, USA. http://www.mts.com (accessed 6-10-2014).
16. Bosch Rexroth AG, Germany. http://www.boschrexroth.com (accessed 6-10-2014).
17. Interface Inc., USA. http://www.interfaceforce.com (accessed 6-10-2014).
18. Servo Innovations LLC, USA. http://www.servotestsystems.com (accessed 6-10-2014).
19. Dassault Systèmes, France. http://www.3ds.com/products-services/simulia/portfolio/abaqus/overview/ (accessed 2-7-2014).
20. Photron Limited, Japan. http://www.photron.com/ (accessed 3-7-2014).
21. Peekel Instruments B.V., the Nethelands. http://www.peekel.nl (accessed 6-10-2014).
22. Lekhnitiskii SG. *Anisotropic Plates*. Translated from the 2nd Russian edition by SW Tsai and T Cheron, 1968, Gordon and Brache, London, 1956.
23. Jong TD. *On the Calculation of Stresses in Pin-Loaded Anisotropic Plates*. PhD dissertation, Delft University of Technology, 1987.
24. Waszczak JP and Cruse TA. A Synthesis Procedure for Mechanically Fastened Joints in Advanced Composite Materials. *Air Force Materials Laboratory Report* 1973; TR-73-145, Vol. II.
25. Garbo SP and Ogonowski JM. Effect of Variances and Manufacturing Tolerances on the Design Strength and Life of Mechanically Fastened Composite Joints. *Flight Dynamics Laboratory, Air Force Wright Aeronautical Laboratories, Technical Report* 1981; AFWAL-TR-31-3041.
26. Whitney JM and Nuismer RJ. Stress Fracture Criteria for Laminated Composites Containing Stress Concentrations. *Journal of Composite Materials* 1974; 8(3): 253–265.

27. VDI. Development of Fibre-Reinforces Plastics Components, Analysis. *VDI Guideline 2014 Part 3*, (bilingual, German and English), Beuth-Verlag, Berlin, 2006.

NLR

Anthony Fokkerweg 2
1059 CM Amsterdam, The Netherlands
p) +31 88 511 3113 f) +31 88 511 3210
e) info@nlr.nl i) www.nlr.nl